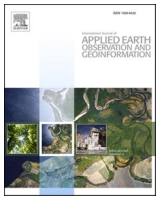
International Journal of Applied Earth Observation and Geoinformation 154 (2026) 105630



Contents lists available at ScienceDirect

International Journal of Applied Earth Observation and Geoinformation

journal homepage: www.elsevier.com/locate/jag



Satellite-based coastal monitoring through variance image composites (*SatVar*)

Pilar Martín-Gallego [a,*], Juan Montes [a], Irene Delgado-Fernandez [a], Laura del Río [a], Theocharis A. Plomaritis [b], Christopher Marston [c]

[a] University of Cádiz, INMAR, Dept. Earth Sciences, Puerto Real (Cádiz) 11519, Spain
[b] University of Cádiz, INMAR, Dept. Applied Physics, Puerto Real (Cádiz) 11519, Spain
[c] UK Centre for Ecology & Hydrology, Library Ave, Bailrigg, Lancaster LA1 4AP, UK

ARTICLE INFO

Keywords:
High variability zones
Satellite derived shorelines
Coastal evolution
Google Earth Engine
Sentinel-2
Image collection compositing

ABSTRACT

The past decade has seen rapid advancements in satellite remote sensing data availability and analysis. In coastal environments, this has enabled regional to global assessments of shoreline trends, a key practical application for management and planning. However, coastal zones are inherently dynamic, while instantaneous shorelines only capture the state of the system at a particular moment in time. This study introduces a novel approach for monitoring dynamic coastal environments using satellite imagery, adapting the principle from ground-based video monitoring systems. The *SatVar* approach presented here uses freely available, medium resolution satellite imagery and Google Earth Engine. The method takes advantage of the increasing availability of cost-free Sentinel-2 imagery and the flexibility of collections acquired over different time periods to automatically detect highly dynamic zones through variance composites, image compositing and segmentation to obtain medium-term trends of coastal dynamics. Natural boundaries are rarely abrupt, so a zone-based (instead of a line-based) approach provides more nuanced information about transitional zones. The identified highly dynamic zones correspond to morphological processes described in literature, and are also used for shoreline extraction. This combined information can enrich understanding of coastal dynamics and overcome some of the limitations of instantaneous shorelines. The approach is tested at three locations with different morphodynamic characteristics and tidal regimes: Sancti Petri (Spain, mesotidal), Narrabeen (Australia, microtidal) and Sefton (UK, macrotidal). Potential applications to monitor changes outside the upper shoreface such as coastal dune dynamics or back-barrier environments are also discussed.

1. Introduction

Satellite-based coastal monitoring has mostly focused on coastline extraction (Splinter et al., 2018; Aghdami-Nia et al., 2022; Chen et al., 2022; Graffin et al., 2025; Martín-Gallego et al., 2025; Zhang et al., 2025, Hung and Tsai, 2026). Recently, several coastline extraction tools have been developed, such as ShorelineMonitor (Luijendijk et al., 2018), CoastSat (Vos et al., 2019), SHOREX (Sánchez-García et al., 2020), CASSIE (Almeida et al., 2021), High-tide SDS (Mao et al., 2021), and SAET (Palomar-Vázquez et al., 2023). Their accuracy varies depending on beach type and tidal range (Vos et al., 2023), and their use in management applications such as assessing coastal adaptation to sea-level rise requires caution because changes to shoreline position reflect a complex interplay of multiple factors influencing the littoral sediment budget (e.g. Davidson-Arnott and Bauer, 2021). Most methods to extract satellite derived shorelines (SDS) rely on single-date images and pixel-based classification, often aided by spectral indices such as the Mean Normalized Difference Water Index (MNDWI). Instant waterline positions refer to a specific moment in time and thus may not be representative of the shoreline position, because both water levels and beach morphology vary across temporal scales (from instantaneous swash movements to seasonal changes to the beach face). Moreover, visually discernible features such as the wet/dry line can vary daily due to tidal and weather conditions, potentially leading to inconsistencies in shoreline position data (Fletcher et al., 2003). Furthermore, individual satellite images can be affected by cloud cover, whitecaps, or sunlight that limit the extraction of shorelines. To address these limitations and account for dynamic changes, the use of composites from multi-date

* Corresponding author.
E-mail address: pilar.martin@uca.es (P. Martín-Gallego).

https://doi.org/10.1016/j.jag.2026.105630
Received 18 February 2026; Received in revised form 18 September 2026; Accepted 28 September 2026
Available online 3 October 2026
1569-8432/© 2026 The Authors. Published by Elsevier B.V. This is an open access article under the CC BY-NC license (http://creativecommons.org/licenses/by-nc/4.0/).

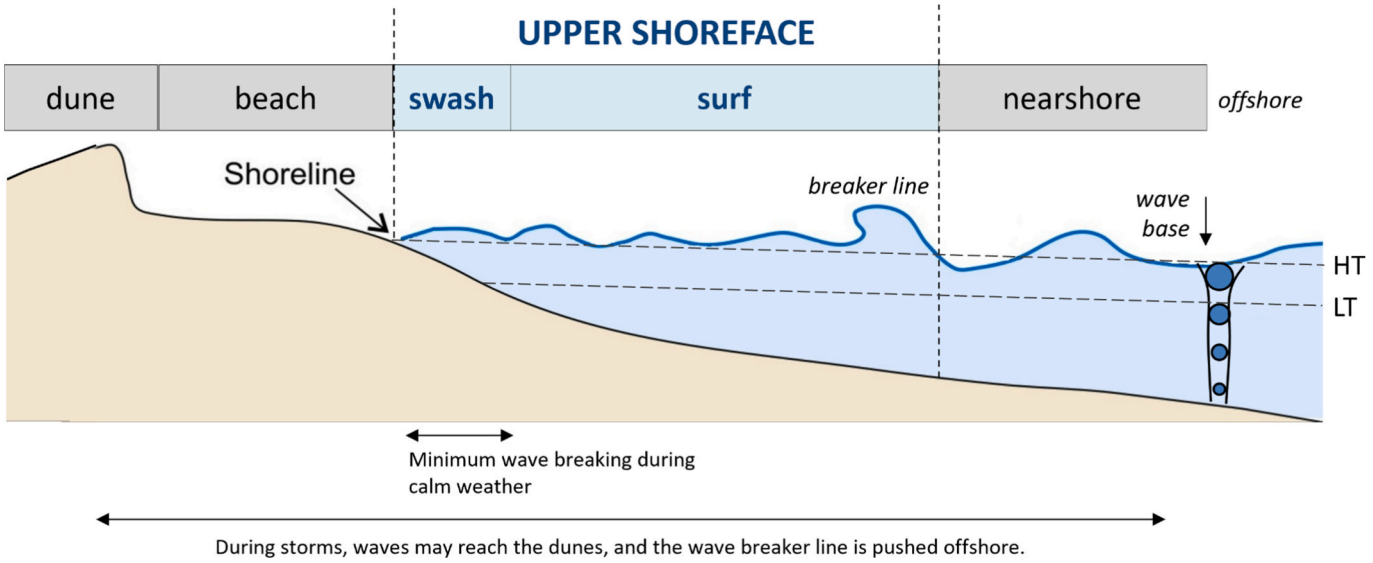


Fig. 1. Simplified beach-dune cross-section to contextualise the "shoreline", with no intertidal bars, and a medium-sized surf zone. HT: High tide; LT: low tide. Modified from Davidson-Arnott et al. (2010).

imagery acquired over a defined period has emerged as a robust approach (Bishop-Taylor et al., 2021; Luijendijk et al., 2018). This method commonly involves median or percentile compositing of image collections, construction of spectral indices, and segmentation of the resulting composite image (Almeida et al., 2021; Bishop-Taylor et al., 2021; Donchyts et al., 2016; Luijendijk et al., 2018; Mao et al., 2021).

The concept of coastline is highly variable and context-dependent, reflecting the dynamic and multidimensional nature of coastal systems and the focus of scientific disciplines, with each definition requiring appropriate proxies or indicators. Determining the coastline location and how it changes is a fundamental variable to understand coastal zones and for management. Coastline movement and its interaction with dunes is key to understanding coastal sandy system evolution (Short and Hesp, 1982; Sherman & Bauer, 1993). Coastlines are less dynamic in cliffs and rocky shores, but their identification is again an important objective of applied research (Trenhaile, 1987). Coastline location and dynamism is equally relevant when studying mangrove forests (Woodroffe et al., 2016), barrier systems (Houser et al., 2008), salt-marshes (Farris et al., 2019) and other coastal habitats. Consequently, multiple reference lines can be used to represent average coastline positions over time. These include geomorphological proxies such as the cliff edge, dune toe, or vegetation limit (Boak & Turner, 2005; Moore, 2000), and hydrodynamic proxies such as mean sea level, and mean high or low water level (Pajak & Leatherman, 2002). The performance of each proxy varies depending on the application. Each proxy and the methods used to identify them come with their own limitations, including issues of data availability and inconsistent definitions (e.g. Boak and Turner, 2005; Smith et al., 2020; Nasir et al., 2022). Additionally, the representation of a dune toe or shoreline as a 'line' is a necessary abstraction for mapping purposes, but it oversimplifies features that are naturally diffuse and spatiotemporally variable.

Regardless of the specific line-based proxy used, this represents just one of the many dynamic features that can be monitored within the coastal zone. The definition of 'coast' itself varies depending on the temporal scale considered. For most applications, the coastal zone is typically defined by the extent of currently active coastal processes (Fig. 1). The shoreline is the intercept of the water level and the beach surface that is migrating offshore and onshore with the tide. In addition, swash motion affects shoreline position at shorter time-scales.

The upper shoreface (Fig. 1), including the surf zone and swash zone, is highly dynamic at short time scales (hours to days). During storms, the breaker line shifts offshore, and storm surge can inundate the beach and

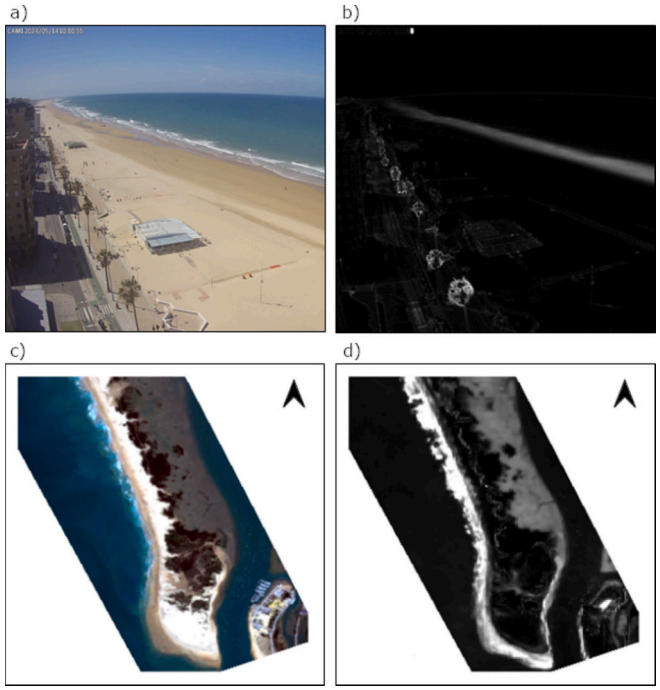


Fig. 2. Examples of a) a snapshot and b) a sigma image extracted from a video monitoring station at Victoria Beach vs. c) median and d) variance composites derived from a GEE collection at Sancti Petri sandspit. Both sites are in the province of Cadiz, SW Spain.

lead to dune scarping by waves. In contrast, under calm conditions, the surf zone may become negligible, with small waves breaking in the swash zone. Satellites overpassing the same location over time should detect these changes, particularly in the upper shoreface where variability is greatest. A pixel's spectral signal may vary quickly and significantly depending on hydrodynamic (wave, tide) and morphological (topobathymetrical) conditions; the same pixel can show water with or without wave breaking, water-saturated sand or dry sand. To capture this dynamism, we introduce a novel methodology: *SatVar*. This method detects high-variability pixels along the coast using medium-resolution (Sentinel-2) multi-temporal satellite image collections analysed using

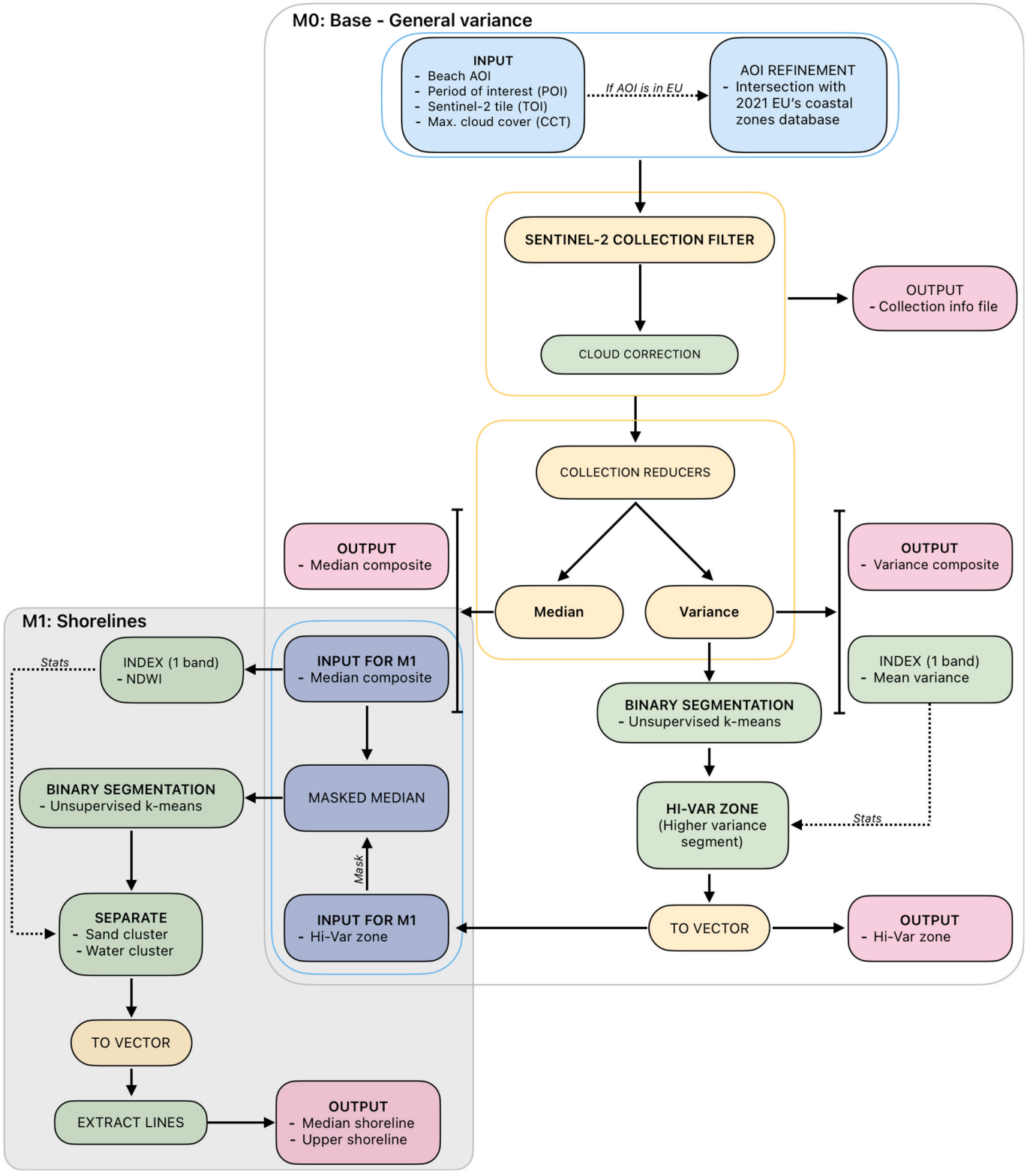


Fig. 3. Overall workflow to detect Hi-Var zones and shorelines from satellite image collections.

Google Earth Engine (GEE; Gorelick et al., 2017), to generate variance image composites over pre-defined time periods (Fig. 2). The principle is similar to the use of 'variance' images derived from beach video monitoring systems (Vousdoukas et al., 2011). Unlike the instantaneous shoreline position, the band comprising the high variability pixels represents a highly variable zone within the beach where most activity is located. This includes the interphase between land and ocean, shaped by tidal and wave-induced displacements along the beach profile, alternating over time between water-covered areas and exposed land, and encompasses the area where the shoreline is likely to be located over a defined time period.

This study addresses the following research questions: i) Can *SatVar* be used to identify high-variability (*Hi-Var*) zones along the coast?; ii) Do these Hi-Var zones correspond to the upper shoreface, as

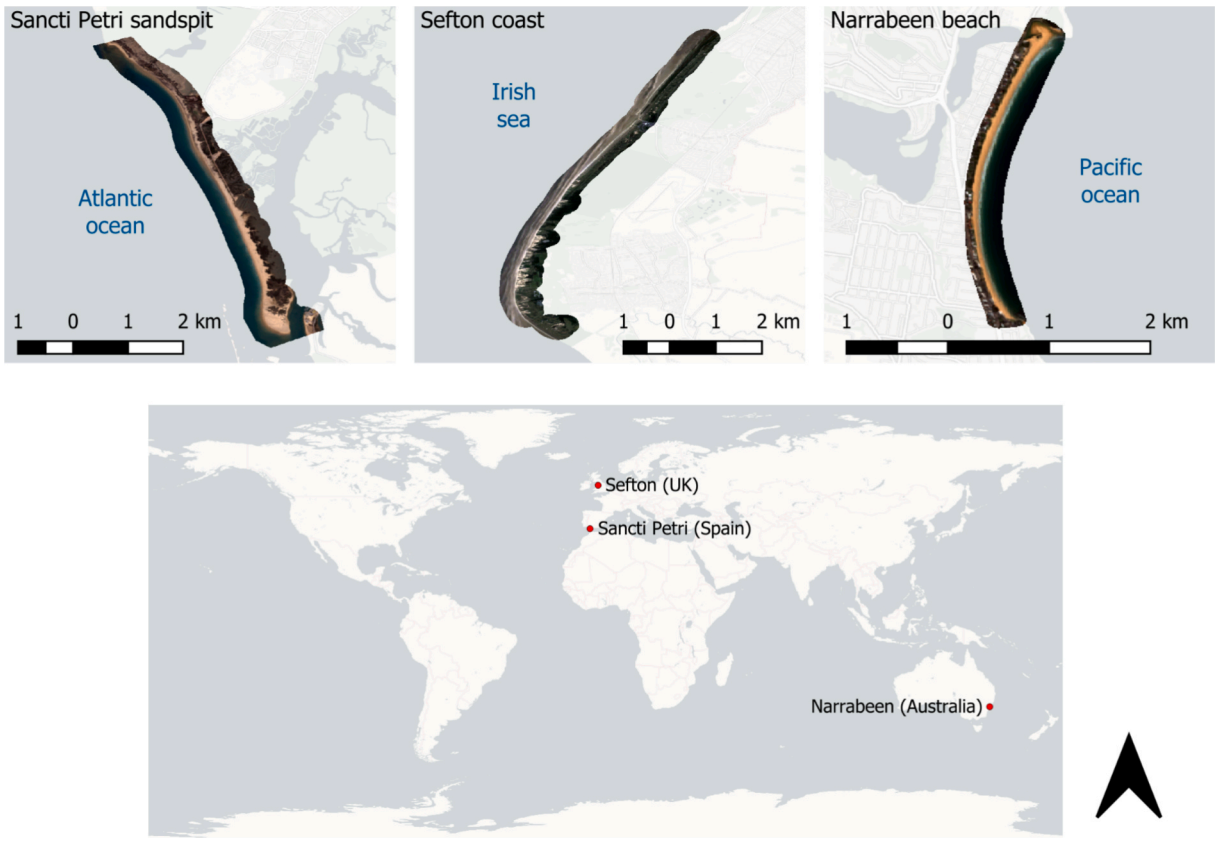


Fig. 4. Study zones: Sancti Petri sandspit (Cádiz, Spain), the Sefton coast (Merseyside, UK), Narrabeen beach (Sydney, Australia) and their locations. Basemap by CartoDB, under CC BY 3.0. Data by OpenStreetMap, under ODbL.

conceptually illustrated in Fig. 1? In theory, the extracted Hi-Var zones should encompass the area within which the shoreline fluctuates over the defined time period, as some of the pixels alternate between water and exposed sand due to tidal and swash movements. Therefore, iii) Can *SatVar* be further applied to extract a representative shoreline from these Hi-Var zones?; and iv) How does the resulting shoreline compare with those derived from existing extraction methods?

These research questions support the aims of this study, which are twofold: 1) To introduce *SatVar*, a tool designed for the automatic detection of highly variable zones and shorelines from multi-temporal satellite image collections on a medium-term scale; 2) To evaluate the performance of *SatVar* in three coastal environments with different tide and exposure conditions by comparing the outputs to SDS derived from other established shoreline detection algorithms.

2. Methodology

2.1. High-Variability zones and shoreline extraction

SatVar has been developed on GEE, and it uses a large number of Sentinel-2 satellite images (an image collection) of a study area acquired over a defined time period. The *SatVar* GEE code and general user instructions can be downloaded from Zenodo (https://doi.org/10.5281/zenodo.17898098).

SatVar is divided into two modules: the base variance module (M0: Base – General variance) and module 1 for shoreline extraction (M1: Shorelines). The M0 (base) generates a table with metadata about the satellite image collection, median and variance composites including all Sentinel-2 original bands, and the Hi-Var zone as output files. The median composite and the Hi-Var zone are required as inputs for M1 (shorelines). User input, which introduces subjectivity and bias, is kept to a minimum.

The M0 requires definition of an Area of Interest (AOI), a period of interest (POI), the Sentinel-2 tile that the AOI falls within (TOI), and a maximum cloud cover threshold (CCT) for image selection. The input AOI is used to select the intersecting beach using the European Union's coastal zones database (Copernicus Land Monitoring Service, 2021) and clip it to the overlapping area, as used in other tools (Palomar-Vázquez et al., 2023). The user may also choose not to employ this database, allowing the use of *SatVar* for beaches with particular geomorphological characteristics, for locations outside of Europe, or for different applications. The advanced settings let experienced users choose between the type of clustering method (K-means or K-means++) and the number of clusters (the default is 2).

Sensitivity analysis to clustering initialization shows statistically similar results for K-means and K-means++, with high stability for $K = 2$ and $K = 3$ (Fig. A.5). Clustering is performed on the S2 composite variance bands, which show similar signals across most bands. Therefore, the problem is effectively low-dimensional and strongly constrained, making a two-cluster framework a natural and physically meaningful approach to distinguish between low- and high-variability zones. More complex environments may exhibit more nuanced variability patterns, and in some cases, a slightly higher number of clusters (e.g., $K = 3$) may capture additional structure in the variability signal and yield marginally improved clustering performance, generally subdividing the high variance cluster, depending on site-specific conditions.

The Sentinel-2 image collection is filtered using the AOI, POI, TOI and CCT. Any remaining cloud influences are removed using the cloud correction algorithm CloudScore + and quality assessment bands (Pasquarella et al., 2023). The collection is then reduced to two composite images using a median and a variance reducer. These reducers calculate a statistic (median or variance) for each band in each specific pixel across the dataset, reducing the entire collection to a single image where the value of each pixel reflects the computed statistic at that pixel

location. Median composite images are widely used in land cover classification studies (Almeida et al., 2021; Bishop-Taylor et al., 2021; Donchyts et al., 2016; Luijendijk et al., 2018; Mao et al., 2021; Marston et al., 2023). In this study, the variance image is used to capture pixel reflectance variability and to identify a Hi-Var zone. The Hi-Var zone is segmented using a K-means clustering algorithm (Arthur and Vassilvitskii, 2007), an unsupervised approach that binarizes the variance image into high and low variability clusters. The vectorised high variability cluster forms the Hi-Var zone polygon.

The shoreline extraction module (M1) extracts two types of SDS from within the Hi-Var zone generated in the M0: a median SDS (or waterline) and an upper SDS. To obtain these, the median composite is masked using the Hi-Var zone and segmented using a k-means algorithm to generate a binary image with two clusters: water and sand/land. A Normalized Difference Water Index (NDWI) is used to identify and label each cluster (McFeeters, 1996). Subsequently, the clusters are vectorised to extract the SDS. The median SDS is the limit between the water and the sand clusters, which identify a water-dominated area, and a sand-dominated area. The water-dominated area includes pixels covered by water in more than half of the images of the collection (i.e., pixels appearing as water in the median composite); the sand-dominated area consists of pixels that remain uncovered by water (i.e., they appear as sand in the median composite). The median SDS consequently represents the waterline in the median composite image. The upper SDS is the upper Hi-Var polygon boundary, and it marks the landward transition from the high variability zone (i.e., the swash zone) to the subaerial beach surface.

Additional to Hi-Var zones and median/upper shorelines, the tool outputs relevant metadata such as the number of images filtered into the image collection, their dates, acquisition times, and cloud cover proportion. This information is key for interpreting results and seasonal biases in the dataset. Fig. 3 summarises *SatVar's* general workflow.

2.2. Test case studies

SatVar was tested at three locations with different morphodynamic characteristics. For this study, the POI was defined as one calendar year, in line with previous studies and to reduce the influence of short-term temporal variability, seasonality and cloud cover in SDS (Almonacid-Caballer et al., 2016; Hagenaars et al., 2018; Luijendijk et al., 2018). The analysed years were 2017–2024. A maximum CCT of 25% was adopted, whereby images containing greater than 25% cloud cover are removed from the image collection; this threshold is highly case-dependent and reflects the need to minimize cloud cover while retaining as many images as possible. Earlier shoreline detection research has used CCTs ranging from 10% to 50% (Billet et al., 2024; Cabezas-Rabadán et al., 2024; Curoy et al., 2022). In regions with frequent cloud cover, higher CCT helps increase the number of usable images, which is important for statistical significance. Users should be aware, however, that a high CCT can lead to artifacts in the output variance composite (e.g. with some pixel locations showing large variability due to frequent cloud cover instead of landscape changes).

2.2.1. Study zones

SatVar was tested in three locations (Fig. 4): the Sancti Petri sandspit (Cádiz, Spain), the Sefton coast (Merseyside, UK), and Narrabeen beach (Sydney, Australia).

Sancti Petri sandspit is a sandy barrier system located in Cádiz, on the southwestern coast of Spain, extending 7 km alongshore in a NW-SE orientation. Its tidal regime is semidiurnal and mesotidal, with mean spring tidal range of 1.20 m and 2.96 m (Benavente et al., 2013). The spit is sheltered by a discontinuous, shore-parallel submerged rocky shoal (Fernández-Montblanc et al., 2018), that becomes shallow enough to outcrop in the intertidal zone at the northernmost end. There is extensive availability of previous field and remote sensing data (Benavente et al., 2013; Del Río et al., 2012; Montes et al., 2024; Poizot et al., 2013; Puig et al., 2016; Talavera et al., 2018,).

The Sefton coast stretches for 36 km in a SW-NE direction in the Liverpool Bay, in northwest England, with a semidiurnal macro-tidal regime reaching a mean spring tidal range of 8.2 m in some locations (Dissanayake et al., 2014). The beach presents complex morphologies in the intertidal area, like well developed ridges and runnels (Pye and Blott, 2008; Esteves et al., 2012). This coast hosts the largest coastal dune field in England, which is subject to erosion and intense human pressure (Dissanayake et al., 2014; Delgado-Fernandez et al., 2019).

Narrabeen beach is a 3.6 km long sandy beach located in Sydney, on the southeastern coast of Australia. The tide regime is semidiurnal and microtidal, with a mean spring tide range of 1.3 m (Ibaceta et al., 2023). Narrabeen is a well-known coastal monitoring site, with periodic beach surveying since 1976, and has been used previously in remote sensing studies (Splinter et al., 2018; Vos et al., 2019; 2023).

2.2.2. Consistency of SatVar performance with other tools

Assessing the accuracy of the detected Hi-Var zones using ground-truth is challenging, as they do not represent a variable that is directly identifiable in the field at a particular time due to the use of image composites. Instead, Hi-Var zones indicate an area of high variability within which most instantaneous shorelines should be located. Consequently, the representativeness of the extracted Hi-Var zones was tested by comparison with a set of shorelines extracted using two widely applied shoreline extraction algorithms: CoastSat (Vos et al., 2019) and the Shoreline Analysis and Extraction Tool (SAET) (Palomar-Vázquez et al., 2023). Both algorithms allow for different configurations depending on the characteristics of the study area and have previously been applied to beaches similar to those where *SatVar* was tested, demonstrating its ability to provide a robust and accurate definition of SDS (Vos et al., 2019; Cabezas-Rabadán et al., 2024) and to capture seasonal coastal processes (Vos et al., 2023). An instantaneous SDS point extracted from any single image (as extracted by SAET/CoastSat) should, by definition, fall within the Hi-Var zone envelope, but not necessarily at a fixed position within it. Its exact location depends on the wave and tide conditions at the time of image acquisition, ranging from the landward edge of the Hi-Var zone under high energy conditions/high-runup and tidal range conditions towards more seaward positions under calm/low tidal range conditions. This means that a high percentage of SDS points falling within the Hi-Var zone is the expected outcome, since the zone is designed to capture the full range of shoreline positions rather than a single, fixed contour.

CoastSat was applied using the default settings, with a reference shoreline and a maximum distance parameter adapted to match European Union's coastal zones database (Copernicus Land Monitoring Service, 2021) used by both SatVar and SAET, ensuring comparability between the different approaches. For the Narrabeen test case, a polygon with the same characteristics as those in this layer was generated, as it was not included in the original dataset. The SAET configuration applied in the three study sites was AWEInsh index with thresholding = 0 and a 3×3 kernel size, with an additional erosion morphological filter used for the Sancti Petri sandspit. This setup was successfully used in previous studies conducted in nearby areas with similar characteristics to Sancti Petri sandspit (Cabezas-Rabadán et al., 2024). For Narrabeen and Sefton, the configuration follows previously implemented applications on the same site or on beaches exhibiting similar characteristics (Vos et al., 2023). Not all the images used for the extraction of the Hi-Var areas were used for shoreline extraction with SAET, as the software was unable to extract the shoreline with the configuration used in some cases.

CoastSat and SAET extract shorelines as both point and polyline features. The yearly SDS datasets in point format were used for comparison with *SatVar*'s Hi-Var zones. For each year (TOI) considered, the proportion of SDS points within the Hi-Var zone was calculated, providing a measure of consistency. Since *SatVar*'s output is an area polygon (the Hi-Var zone), the Hi-Var area was also compared with an envelope polygon including all CoastSat and SAET shorelines to further

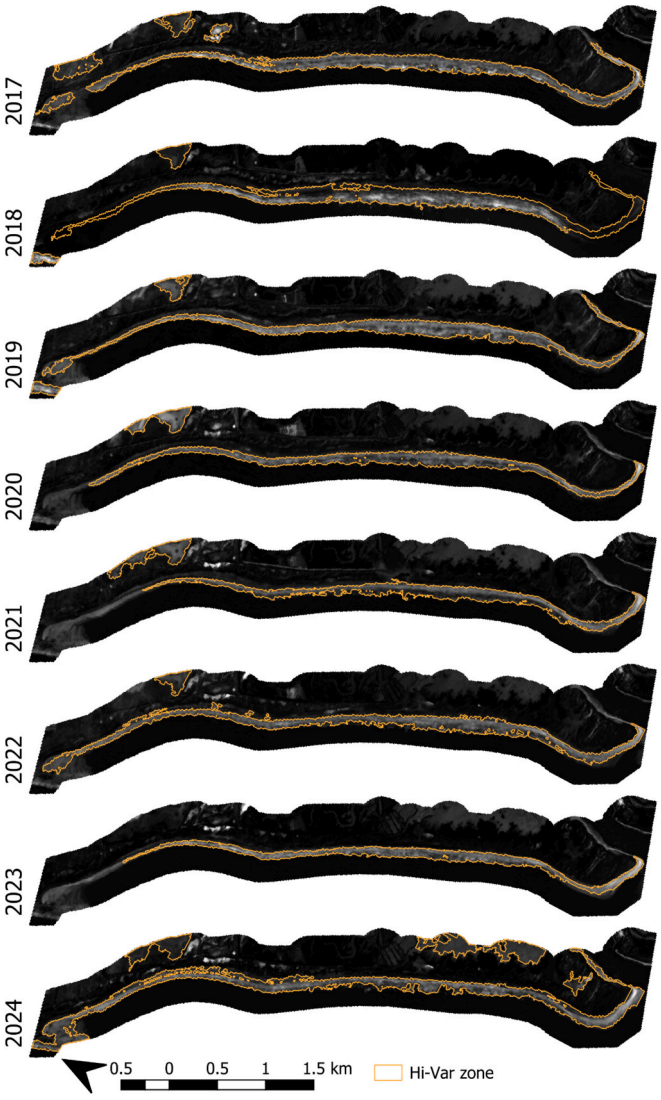


Fig. 5. Hi-Var zones for each year related to the variance image used for the extraction in Sancti Petri sandspit.

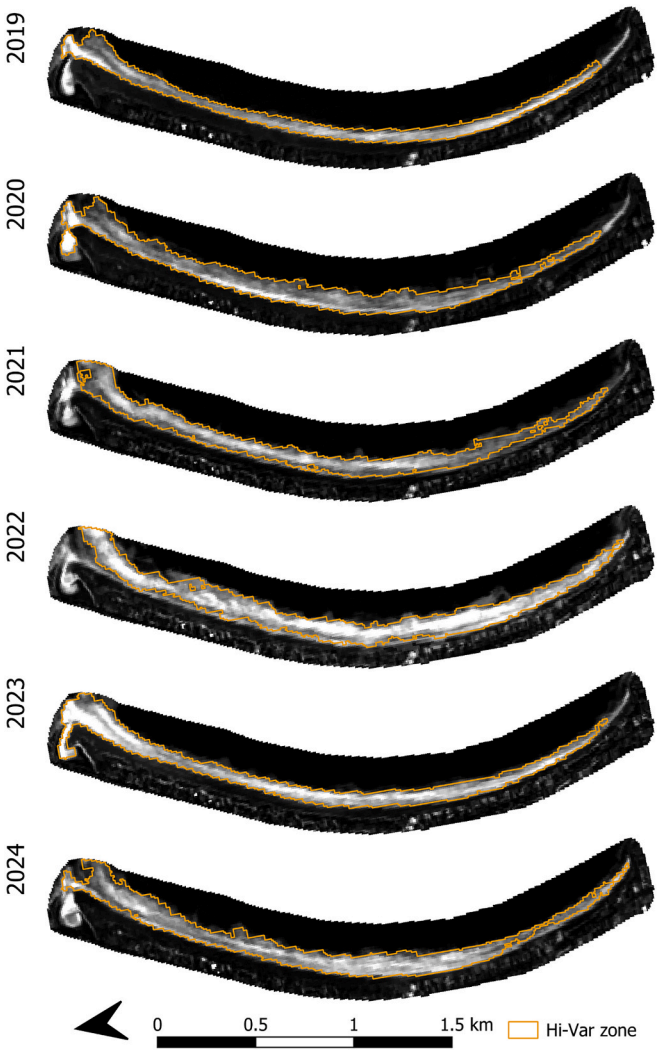


Fig. 7. Hi-Var zones for each year related to the variance image used for the extraction in Narrabeen.

assess the consistency of *SatVar*. Their overlap was calculated to assess Hi-Var zones commission and omission errors compared to both algorithms.

For each study site (Sancti Petri, Narrabeen and Sefton), two years were used for consistency assessment. The choice of years was based on the number of images within the GEE image collection. In each location, the years with most and least images were used to test the performance

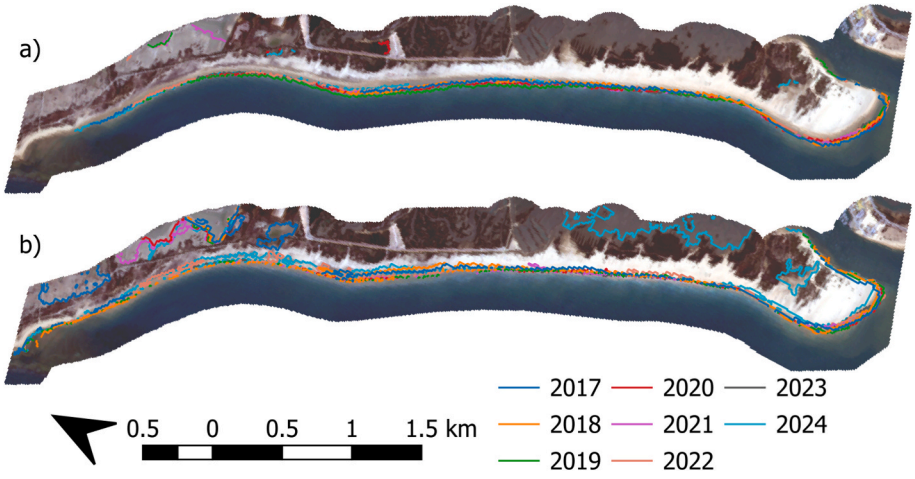


Fig. 6. Median SDS (a) and upper SDS (b) for the Sancti Petri sandspit. The background image corresponds to the median composite for 2024.

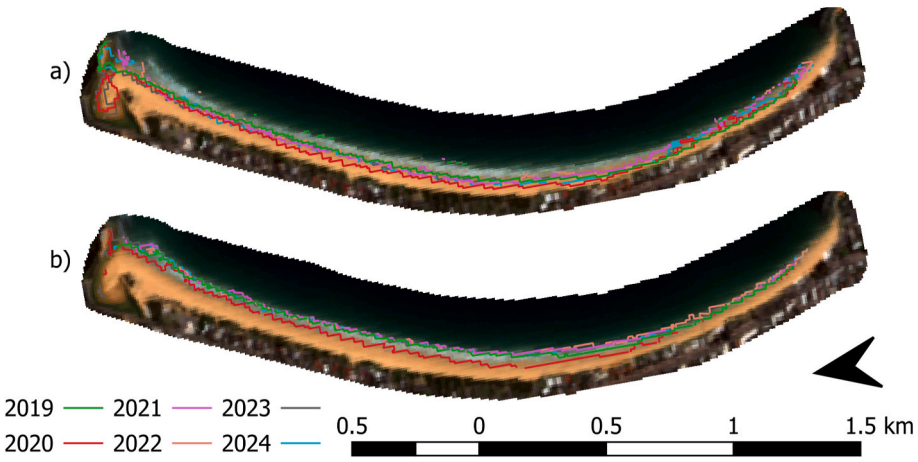


Fig. 8. Median SDS (a) and upper SDS (b) for Narrabeen beach. The background image corresponds to the median composite for 2024.

with the best and most limited scenarios. This results in six years for assessing the performance of *SatVar*.

3. Results

3.1. Hi-Var zones, 'median' and 'upper' SDS

SatVar detected alongshore changes of Hi-Var zones (hotspots of pixel variance) at the three sites. In Sancti Petri (Fig. 5), most Hi-Var zones are concentrated in the upper shoreface, which considerably changed in size alongshore the selected AOI, although some fell outside the beach (e.g. isolated polygons landwards from the dunes). *SatVar* successfully delineated the morphology of the southern end of the spit throughout the POI. The inner part of the tidal channel was identified only in 2017–2019 and 2024. The channel has steep slopes due to periodic dredging leading to intermittent delineation of narrow Hi-Var zones. To the north, the area sheltered by the rocky shoal was not detected as a Hi-Var zone in 2020, 2021 and 2023, preventing the possibility of obtaining shoreline positions in that location.

SatVar successfully identified both the median and upper SDS for most POIs in Sancti Petri (Fig. 6). Median shorelines predominantly appeared within the intertidal zone, without significant anomalous areas in the backshore, while upper shorelines corresponded to the upper limit of the Hi-Var zone. In some sectors, upper SDS were displaced landwards and appeared within the marsh behind the barrier.

Likewise, *SatVar* successfully delineates the upper shoreface in Narrabeen beach (Fig. 7). This appears as a Hi-Var zone that is coherent alongshore throughout the selected POI (2019–2024), reflecting a temporally variable surf zone where regular changes to wave breaking facilitate extraction of high variability pixels from variance composites. Years 2017 and 2018 were excluded from the analysis, as their collections had less than 10 images, being unsuitable to derive a significant variance. Coherent Hi-Var zones lead to effective extraction of the median and upper shorelines (Fig. 8). Similar interannual and spatial variability has been observed using modelling (Ibaceta et al., 2023; Splinter et al., 2014) and field techniques (Harley et al., 2011) at Narrabeen. The interannual variability has been also successfully correlated with large scale climate indices (Harley et al., 2009).

SatVar produces Hi-Var zones that are compartmentalised both cross-shore and alongshore at Sefton (Fig. 9). The irregular variance signal partially reflects a complex, macro-tidal environment where large tidal excursions shift the upper shoreface landwards and seawards by hundreds of meters every day. This generates a segmented variance response as the intertidal zone is inundated and drained, and as waves break on nearshore and intertidal bars at different positions cross-shore. These sandbars are known to generate pixels of changing reflectance due to waves breaking over them (Frugier et al., 2025). The irregular variance signal at Sefton can also be related to dune mobility. Significant dune trampling creates hotspots for variability within the dune area (Delgado-Fernandez et al., 2019), with variance composites picking up signals related to changes to dune landforms, aeolian processes, and the burial and growth of vegetation over time. The interaction between large tidal ranges and dune changes leads to irregular Hi-Var zones (Fig. 9) that limit the possibility of extracting a 'shoreline' (Fig. 10). This limitation also affects other SDS extraction algorithms, which yield high error in macrotidal environments (Graffin et al., 2025). In addition, an instantaneous shoreline extracted in a complex tidal area has a different geomorphological significance than in a microtidal coast (Pardo-Pascual et al., 2012). Hi-Var patterns in complex coastal environments such as Sefton, where a zonal approach might be more appropriate, should be explored in future studies.

3.2. Consistency of SatVar output with other tools

The location of SAET and CoastSat shorelines relative to Hi-Var zones is presented in Figs. 11 and 12 respectively, with a summary of comparative results between SAET/CoastSat and *SatVar* included in Table 1. The performance assessment was done for the years with the largest and smallest GEE image collections. SAET was able to extract shorelines in 91.44% of the images used by *SatVar* (235 vs 257 images, respectively). Conversely, CoastSat extracted shorelines on 303 images. On average, 46.52% of the yearly SAET shoreline points were located within the Hi-Var area polygons, with standard deviations ranging from 12.90 to 39.29 (Table 1). These values were generally lower for CoastSat, with an average of 37.71% of the yearly CoastSat points within the Hi-Var polygons, and 10.12–26.54 standard deviations. To complement the performance assessment, the Hi-Var zones were compared with an envelope polygon including all yearly SAET/CoastSat shorelines (Figs. A.1 and A.2). Over 90% of the Hi-Var zone overlapped the SAET/CoastSat envelopes in most years, reaching 99% in Narrabeen with SAET and Sefton with CoastSat (Table A.1). Consequently, the commission error is very low in all years for the extracted Hi-Var zones. Conversely, the omission error is consistently very high. The proportion of SAET/CoastSat SDS points within the Hi-Var zone indicates good consistency between SatVar and the reference shoreline datasets, since it confirms that the observed range of shoreline positions falls within the envelope of high variability identified by SatVar. Points located outside the zone are more likely to result from (i) SDS extraction errors, particularly at the *meso*-macrotidal sites, or (ii) an incomplete representation of the full range of conditions within the image composite used to derive the Hi-Var zone, rather than indicating that the shoreline is systematically located outside the zone that SatVar is designed to capture.

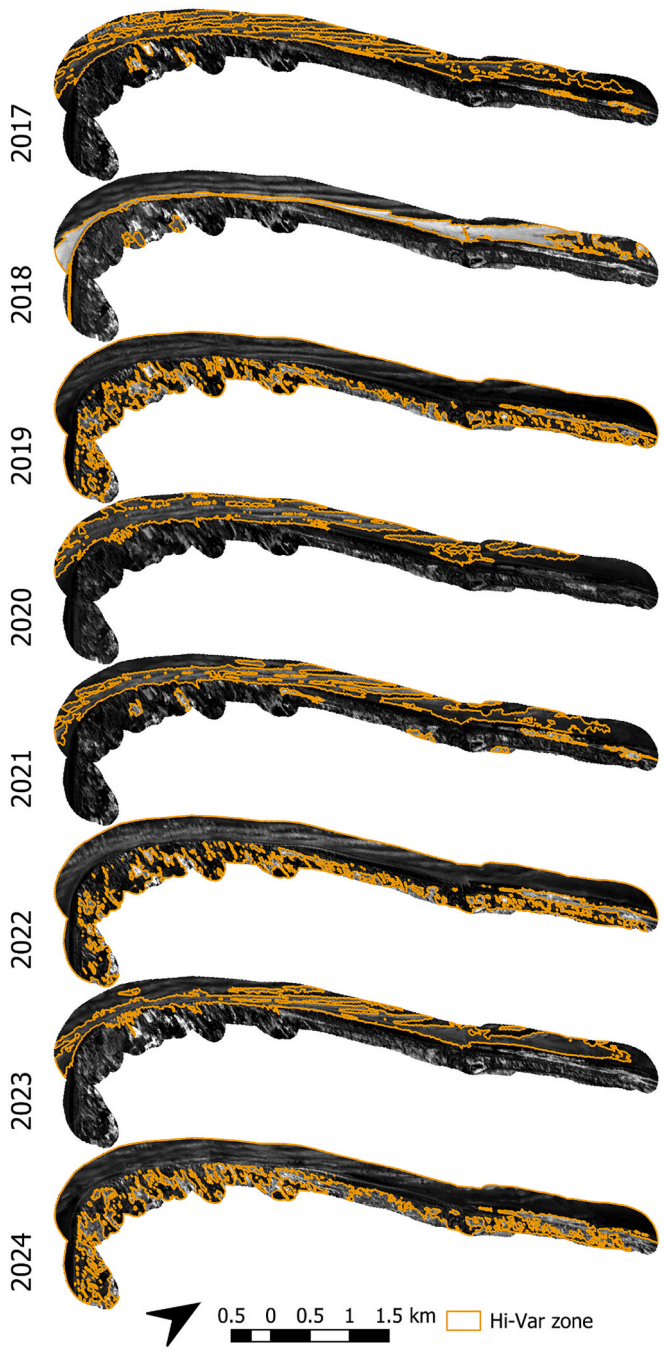


Fig. 9. Hi-Var zones for each year related to the variance image used for the extraction in Sefton.

The saltmarsh area landward of Sancti Petri (see Fig. 4 for context) was consistently detected by SAET and CoastSat but omitted by *SatVar* in most years. Since *SatVar* is based on the variance of the pixel reflectance over a POI, and the reflectance of marsh vegetation pixels does not change as much as the upper shoreface, lower variance marsh pixels are masked out by other pixels in the segmentation. Another difference between the two methods can be observed to the north of Sancti Petri, where SAET and CoastSat extract multiple shorelines exhibiting complex spatial patterns, likely as a result of the presence of the rocky shoal. In Sefton, there are large differences between the two analysed image collections, showing a high sensibility to image availability in *SatVar*. In 2018, the year with the most images in the collection (41 images), the Hi-Var zone is constrained to the coastal area, while SAET identified the shorelines on seaward positions. In 2023, the year with the smallest collection (21 images), SatVar adjusted the Hi-Var zones to the complex morphologies present in the intertidal area, also identifying patches on seaward positions, showing a behaviour similar to SAET. For both years, CoastSat extracts a complicated pattern of shorelines following the complex patterns of the intertidal area and even the dune area. Narrabeen shows a similar behaviour in both years for SAET, with slight differences in the upper part of the beach, where SAET shorelines reach landward positions. For both analysed years, SAET exhibits a double shoreline seaward in several cases, due to the combination of the selected water index and threshold. This is an artifact that diminishes the number of points inside the Hi-Var zones and increases the value of *SatVar*'s omission error, but it could be corrected by filtering SAET's output. CoastSat consistently delineates the northernmost part of Narrabeen beach, where a creek is present. This is not detected by SatVar as it is a sheltered area. Finally, there are other artifacts that generate seawards shorelines in Sancti Petri and Sefton due to the presence of an intertidal rocky platform causing shoreline misinterpretations as a result of tidal and wave oscillations in Sancti Petri, or the large tidal excursion and sandbars in Sefton. This increases the omission error in both sites, as can also be observed in the comparison with the envelope polygon (Figs. A.1 and A.2).

4. Discussion

4.1. Hi-Var zones and SDS with SatVar

Shoreline positions extracted with *SatVar* require an image collection reduced into a single composite. Therefore, *SatVar's* median and upper SDS are not intended to analyse short-term changes such as storm impacts. The upper SDS marks the dominant annual transition from the high variability zone (i.e., the swash zone) to the more stable part of the AOI over each analysed year (i.e., the subaerial beach surface). The median SDS constitutes the dominant shoreline position (land–water boundary) over each analysed year. These composite-based SDS extractions eliminate short-term shoreline variability and provide useful information for mid-term shoreline evolution monitoring (Luijendijk et al., 2018; Bishop-Taylor et al., 2021). Due to the limited historical archive of Sentinel-2 imagery (less than 10 years), a mid-term analysis is not possible. Future work should investigate the use of SatVar on Landsat data to enable a multi-decadal assessment of shoreline (and Hi-Var zone) trends. Annual Hi-Var zones are consistently detected in coastal sites and are useful to identify high variability zones and assess inter-annual variability (research question i). With the limited historical archive of Sentinel-2, this analysis can only be performed from 2017 onwards (2016 if the POI is not a calendar year). Using the Landsat archive would allow including earlier years in the assessment; however, the lower spatial and temporal resolution of Landsat may limit the accuracy and applicability of the method. Available methods to produce sub-pixel resolution SDS contours could be explored to partially overcome this limitation. Earlier studies have shown that sub-pixel contours obtain better results when mapping linear features such as SDS (Vos et al., 2023). However, this requires advanced processing that is not efficient to implement in GEE. Further work could adapt *SatVar* M1 (shorelines) to include smoothing filters.

Single date images provide temporal snapshots of the shoreline position, with the effect of instantaneous water levels and landward offsets due to wave conditions often cited as limitations for improving the accuracy of SDS (Vos et al., 2023). The use of image collections and median or percentile composites introduces a seaward offset in SDS due to wave breaking (Hagenaars et al., 2018). However, as explained in section 1, the ultimate goal of delineating features such as shorelines (or dune toes) on a map leads to reduction and simplification. First, because of all the variability in coastal zones, the shoreline is one of the many dynamic aspects that can be monitored (Fig. 1). Second, because the identification of a shoreline assumes a level of artificial precision that

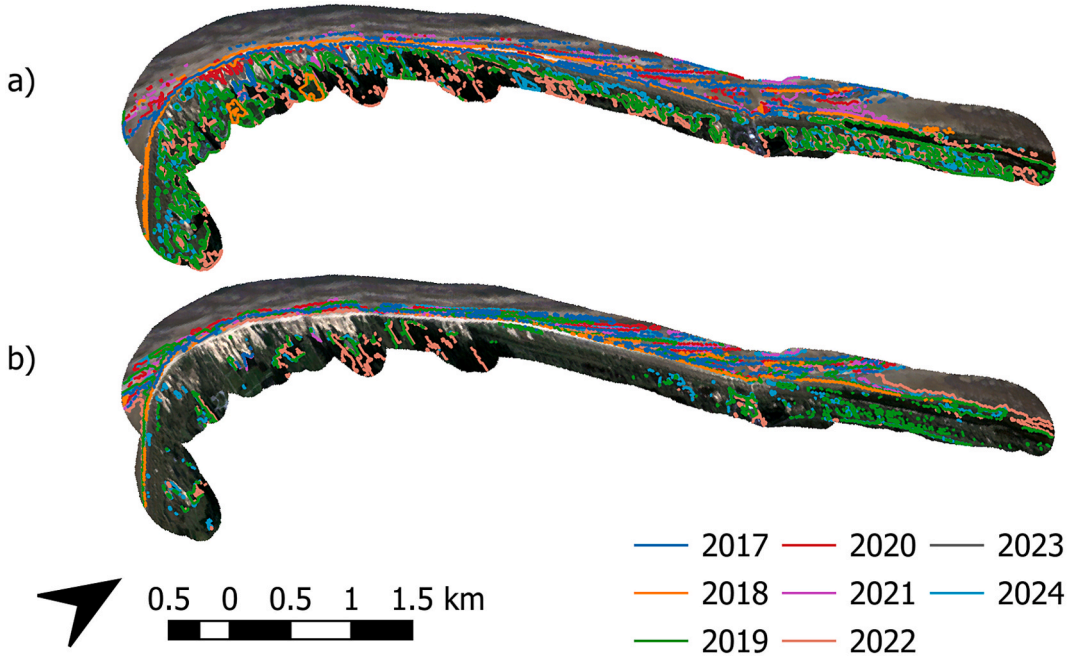


Fig. 10. Median SDS (a) and upper SDS (b) for the Sefton coast. The background image corresponds to the median composite for 2024.

may not reflect the natural variability of these features in the field (Smith et al., 2020). These 'lines' often occupy zones rather than discrete positions, existing as transitional areas with a spatial and temporal variability that cannot be fully captured by a linear feature. In other words, the accuracy implied by drawing a sharp line on a map often exceeds the uncertainty of defining the position of the shoreline in the field. In addition, shoreline changes lead to a landscape reconfiguration of the surrounding land covers (beach, marsh, coastal forest) following complex patterns (Chen & Kirwan, 2022). Presenting this shoreline change as a zone change may help understanding these landscape patterns in coastal ecosystems.

Because of this 'fuzziness of natural boundaries', *SatVar* favours zonation vs. linear approaches. The variance of pixel values in a time series of Sentinel-2 images over a beach captures changes in reflectance caused by the alternating presence of calm water, wave breakers, exposed land, etc. Sentinel-2 images also capture turbidity and high energy conditions, but if these only appear in a limited number of images, their contribution to the variance of the composite is softened. In addition, in many places, storms are associated with cloudy conditions, preventing the use of images coinciding with these events (Vitousek et al., 2023). Instead, Hi-Var zones will include pixel values that change frequently throughout the year due to tides, storms, wave run-up and breaking. This corresponds with the upper shoreface in Sancti Petri and Narrabeen, confirming the research question ii. For Narrabeen, the Hi-Var zone coincides with areas of high vertical profile variability that extends below mean sea level, supporting the identification of the land-sea boundary. The Hi-Var peak is located further offshore, towards the breaking zone, in more dissipative profiles and shifts landward towards the lower intertidal zone in more reflective profiles (Figs. A.6 and A.7). However, Hi-Var zones are statistical descriptors that are subject to site-specific interpretation of the results. Our approach to extracting shoreline positions assumes that Hi-Var zones group the different shorelines for that location over the POI. From this point, the two types of shorelines presented in this article, median and upper SDS, can be extracted (research question iii). Even though Hi-Var zones provide information about coastal processes and allow a better understanding of coastal evolution, shorelines are also extracted for compatibility with other widely applied methods or for management purposes.

Earlier SDS studies employing image collection composites have generated global and continental datasets and have focused on assessing medium-term coastal changes (Luijendijk et al., 2018; Bishop-Taylor et al., 2021; Mao et al., 2021). Using image collections dampens the effect of seasonality and tides in the detected shorelines (Luijendijk et al., 2018), especially if the dates of the images are well distributed throughout the study period. Hence, *SatVar* does not require additional information to correct the effects of tides or wave influences. The statistical compositing of the image collection using the variance and our approach using a shore zone instead of a line is new, and overcomes the main limitation of satellite- derived shoreline studies (i.e. the continuous variability of such line) by shifting the focus from a line to a zone of variation.

Testing the accuracy of SDS and Hi-Var zones is complicated due to the lack of appropriate ground-truth data. Systematic, large scale field surveys synchronized with the passing of Sentinel-2 during a sufficiently long POI would be required for direct field validation of the results of an analysis using image collection composites. SatVar's outputs, being statistical in nature, do not have a direct physical correlation in the field at a particular moment in time, as Hi-Var zones reflect the variation (variance) of pixels over a time period. Consequently, this study has evaluated the approach by comparing SDS extracted from Hi-Var zones with SDS extracted from SAET and CoastSat (research question iv). Results suggest that *SatVar* is capable of differentiating between the upper shoreface and the subaerial beach. Furthermore, *SatVar* could be integrated in workflows with SAET, CoastSat or other shoreline extraction methods for various purposes, such as filtering out spurious results (see Fig. 11), identifying the area of interest, and helping select configuration parameters. Relatively large omission errors obtained from comparing *SatVar's* Hi-Var areas with SAET and CoastSat (Table A.1) point to the main difference between *SatVar's* approach and that of other SDS algorithms. *SatVar* limits the shoreline extraction to the most dynamic part of the beach, while other algorithms use the whole beach. This decreases the detection of false shorelines in tidal environments, while making our approach less sensitive to extreme shoreline locations. Future studies should explore alternative approaches to variance thresholding, including the possibility of using fixed variance values instead of the current automatic segmenting technique. This could help focusing the variance signal on the upper shoreface instead of showing Hi-Var zones in other places such as marshland, but it could

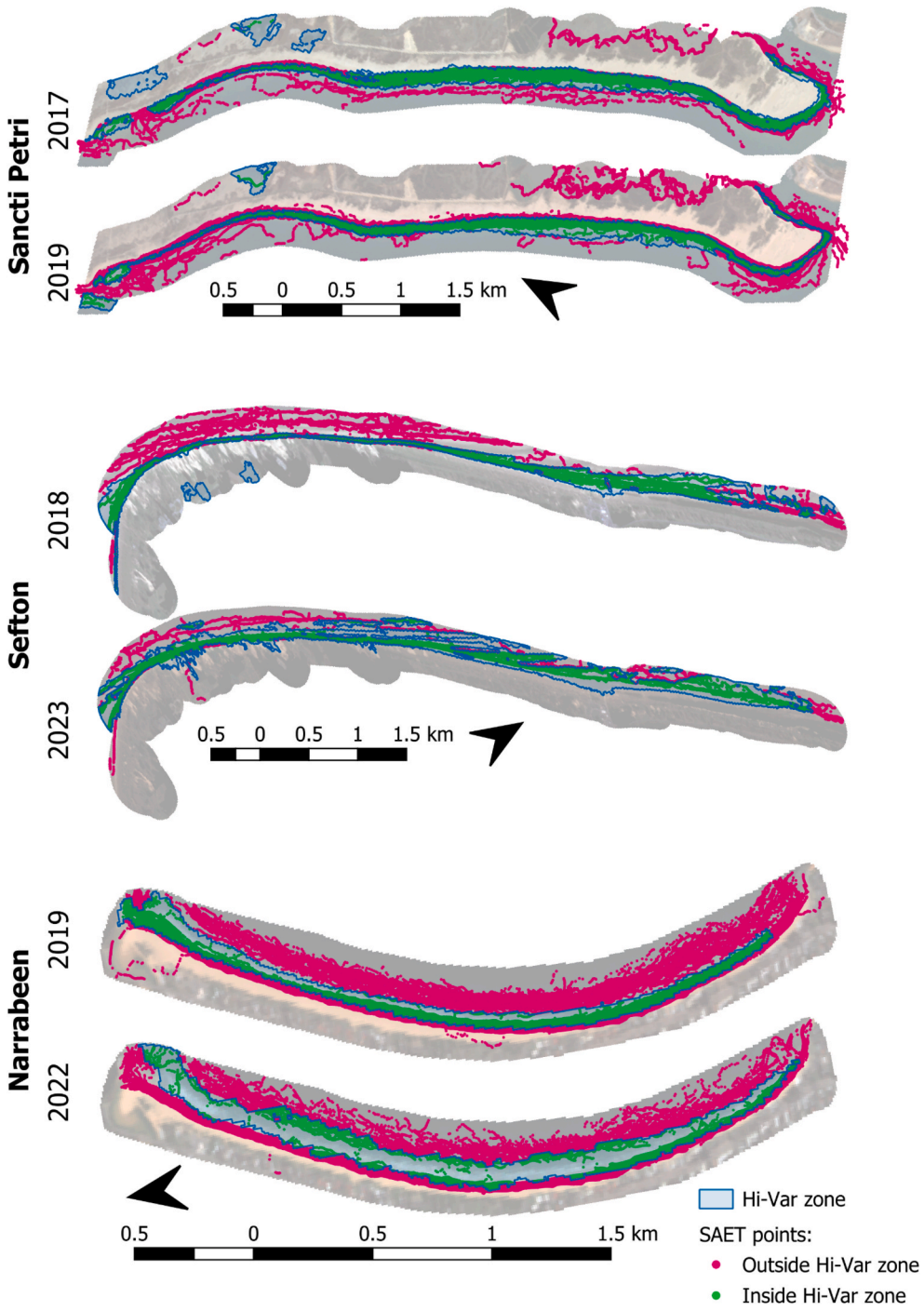


Fig. 11. Comparison between SAET SDS points and Hi-Var zones for performance assessment in the three study sites.

also limit automation. The application of alternative dispersion statistics such as range or interquartile range could also be explored further, as these could improve results on beaches with different hydrodynamic conditions.

4.2. Test case studies: Hi-Var zone interpretation and SDS

The performance of *SatVar* in coastal environments with different characteristics was assessed through the interpretation of the tool's outputs and by comparing it with SAET and CoastSat. *SatVar* is capable of detecting Hi-Var zones or pixel variance hotspots across different types of environments, making its potential applications broad and versatile. These hotspots are located in zones with changing land surface cover. The independent development of the M0 module was conducted based on this premise. For coastal applications, *SatVar* Hi-Var zones correspond to a 'shore influence zone', as in these environments the highest variability is typically found in the upper shoreface area, where pixels rapidly alternate between water with or without wave breaking, water-saturated sand or dry sand depending on wave, tide and beach conditions, and where the instantaneous shorelines are likely to be located over the POI. In turn, the shore influence zone (Hi-Var zone) is strongly influenced by the hydrodynamic and morphological characteristics of the area. A seasonal behaviour of the beach slope causes the shore influence zone to expand or contract accordingly. Furthermore, the presence of rocky platforms also affect the spatial distribution of the variability, increasing the shore influence area under low-tide and high-

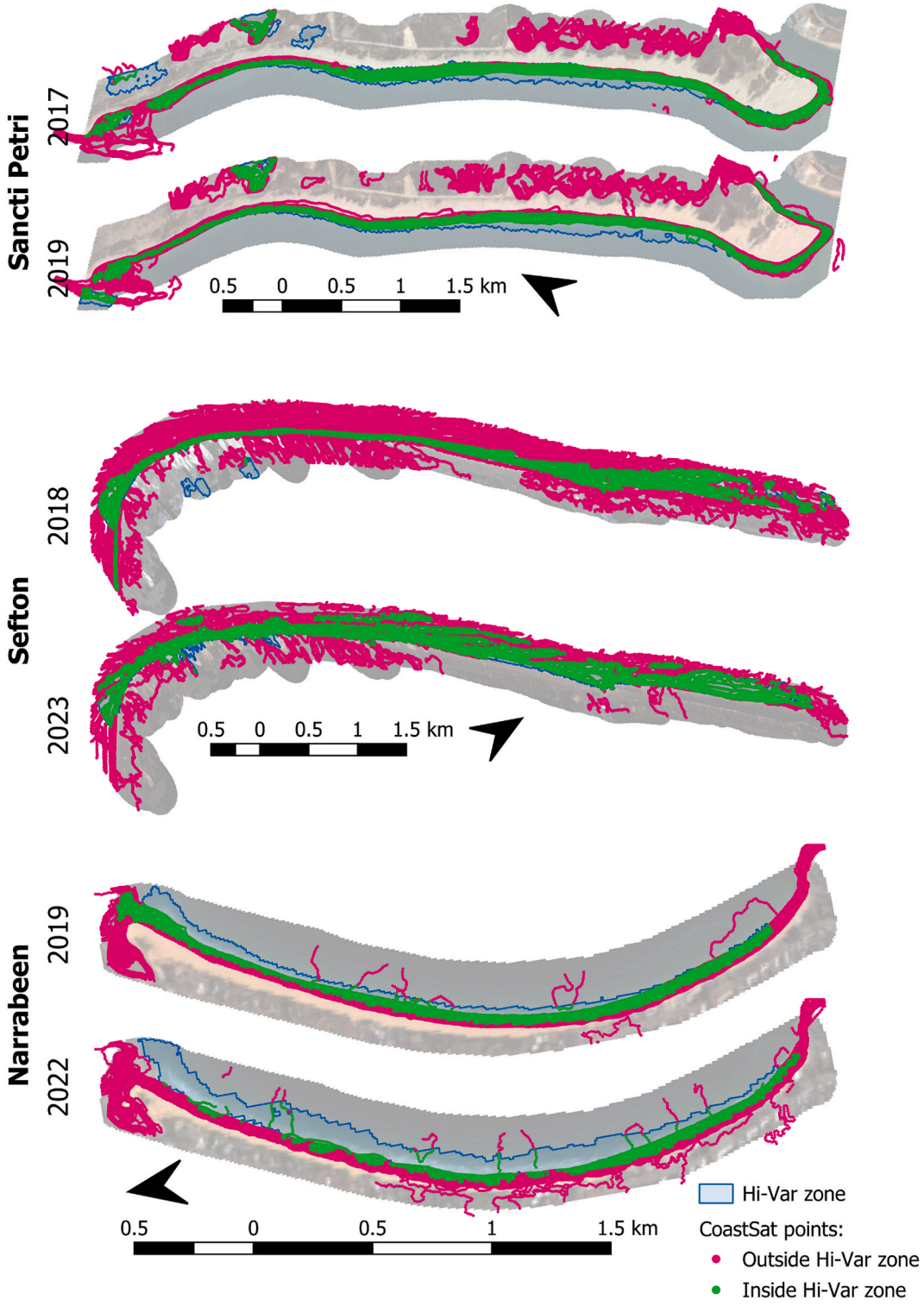


Fig. 12. Comparison between CoastSat SDS points and Hi-Var zones for performance assessment in the three study sites.

wave conditions.

4.3. *SatVar interpretations: Knowing your site*

As described in the previous section, *SatVar* lacks capability to differentiate between the multiple sources of variability. This article interprets Hi-Var zones as representing the "upper shoreface" but results from both Sefton and Sancti Petri show that other processes, such as sandbars, dune mobility, vegetation dynamics, and saltmarsh variability, can also produce high-variance signals (hence the emphasis on site-specific knowledge). Future work could explore options to decrease this ambiguity such as incorporating NDVI time series to identify vegetation-driven variability, or comparing variance patterns across different spectral bands (visible vs. SWIR) to distinguish water-related from vegetation-related changes. In sites with complex morphologies or variability patterns, it might be helpful to explore the advanced *SatVar* initialization settings, which offer the possibility of applying K-means++, optimising the initial placement of centroids for

Table 1
Yearly proportion of SAET/CoastSat extracted SDS points that were located within the Hi-Var area. "Number of images Hi-Var" refers to the number of Sentinel-2 images used by SatVar to generate the annual variance composite (i.e. the Hi-Var zone). The discrepancy in the number of images used for SAET/CoastSat and SatVar arises from differences in data access, preprocessing, and filtering strategies between the Copernicus and GEE catalogues and the pre-filtering of each tool.

Study area	Year	Mean SAET points in Hi-Var zone (%)	Standard deviation (SAET)	Mean CoastSat points in Hi-Var zone (%)	Standard deviation (CoastSat)	Number of images Hi-Var zone	Number of images SAET	Number of images CoastSat
Sancti	**2017**	66.26	22.33	49.06	10.12	20	34	35
Petri	**2019**	54.10	26.58	45.26	17.22	50	47	51
Sefton	**2018**	33.55	39.29	21.76	26.54	41	23	43
	2023	55.93	38.88	39.25	25.04	21	17	31
Narrabeen	**2019**	43.34	23.21	45.30	19.31	79	70	82
	2022	25.92	12.90	25.64	15.75	46	44	61
	MEAN	**46.52**	**27.20**	**37.71**	**19.00**			

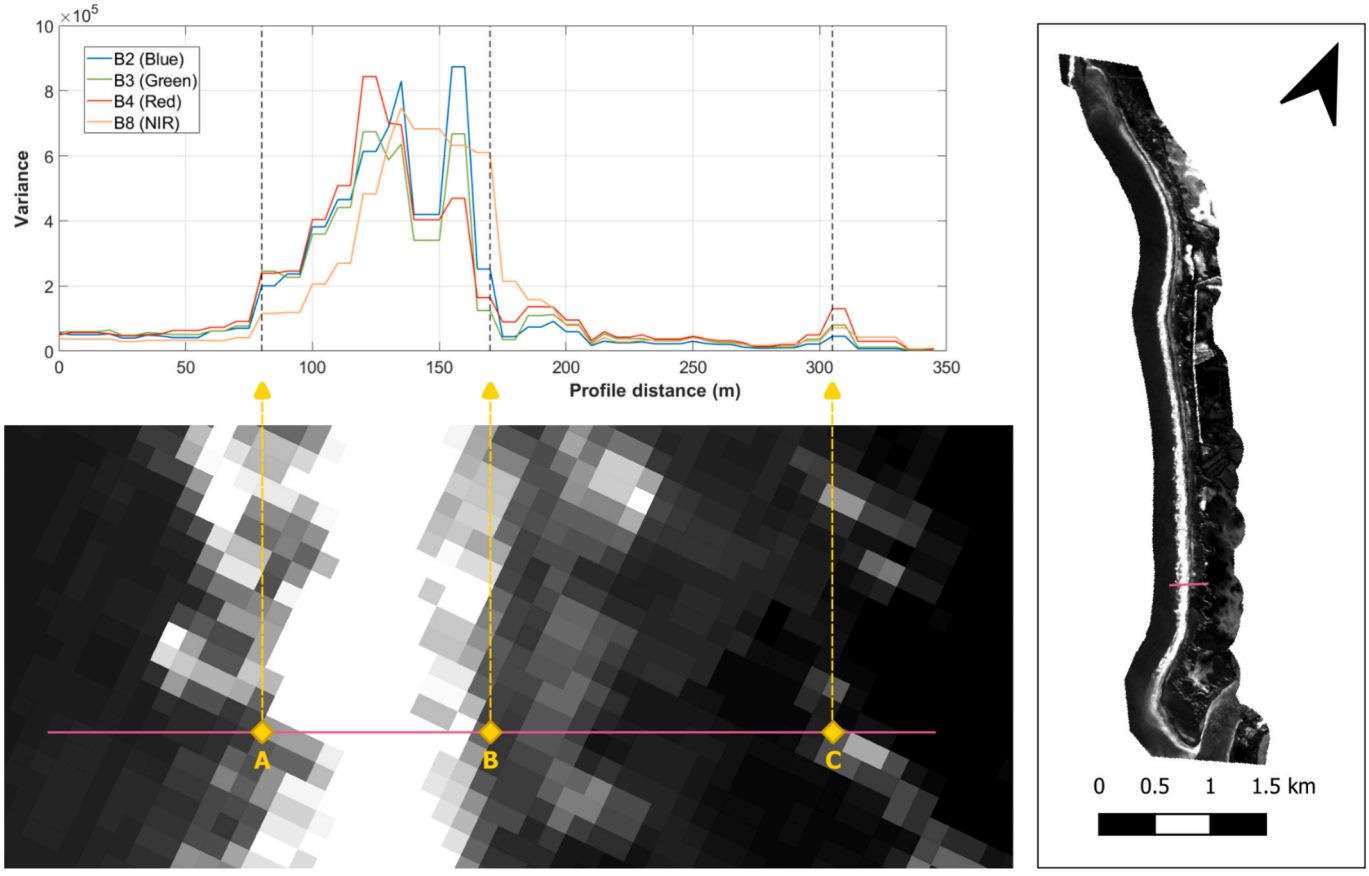


Fig. 13. Variance profile of Sentinel-2 bands B2, B3, B4, and B8 (10 m spatial resolution) over a section of Sancti Petri sandspit, clearly showing the limits of the surf zone (a and b) and a distinct peak in variability associated with the dune area (c).

clustering (Arthur and Vassilvitskii, 2007), and of increasing the number of clusters, providing more nuanced information about land surface variability.

To generate the Hi-Var zone, *SatVar* selects pixels that show large variability throughout the POI. The physical meaning of this variability needs understanding of the perspective of the satellite viewing the site, as well the perspective of the algorithm using available images to create the variance composite itself. The variance reflects both dynamism and change, with automatic segmentation meaning that the output Hi-Var zones are always relative to the values within that composite. For example, when the beach-nearshore system is selected, pixels whose values change the most will likely be those in the surf and swash zone. This leads to *SatVar* performing well when selecting the upper shoreface, because pixel variability in this area is higher in comparison with pixel variability elsewhere on the beach over a full year. The transition from bare sand to a vegetated pixel could, in the absence of waves, become an area of maximum variance and lead to automatic segmentation of a Hi-Var zone in the dunes. Variability changes on the dune system can also be observed in composites showing high variance on the surf and swash zones, although it will be slightly masked by the higher values. This can be seen in Fig. 13, where, in addition to the clear identification of the surf and swash zones, a lower peak in variability is observed coinciding with the beginning of the dune system in Sancti Petri sandspit. Only the bands at 10 m spatial resolution were used, as they are more sensitive to fine scale patterns. The variance profile with all Sentinel-2 bands is shown in Fig. A.3.

The argument above could be applied to other situations, expanding the applicability of *SatVar*. However, this requires local knowledge of the specific AOI, as well as information on the collection and the metadata. For example, the variance composite series in Fig. 5 shows Hi-Var zones landwards of the dune front that correspond to areas of the back-barrier saltmarshes, and Fig. 9 shows the Hi-Var zone delineating

complex morphologies typical of macrotidal environments. This opens the possibility of using *SatVar* to explore hotspots for variability along the entire coast, and initiate analyses of the reasons for that relatively higher variability at segmented locations (e.g., flooding in marshlands).

Similarly, and as mentioned above, exploring the metadata and image collection characteristics is key to adequate interpretation of results. Imagery downloaded from GEE was well distributed throughout the POI in most cases (Fig. A.4). The consistency in both the number and temporal distribution of images per month supports the inter-annual comparability of Hi-Var zones.

Finally, the choice of the most adequate Sentinel-2 bands for each application could be explored in further research, as they could improve the detection of features of interest depending on their reflectivity and size or spatial pattern. On its default setting, and to make it as simple and automatic as possible, *SatVar* uses all Sentinel-2 bands for the calculations.

5. Conclusion

Throughout this research, we have introduced *SatVar,* a Sentinel-2-based tool that uses a freely available routine in GEE to identify high-variability (Hi-Var) zones. Although initially conceived and tested for coastal applications, *SatVar*'s variance approach using GEE image collections (M0: Base) could be applied in other environments or transitional zones subject to land surface variability. *SatVar* is an exploratory tool for identifying zones of change, not a deterministic monitoring tool. The physical meaning of the Hi-Var zone is case-dependent, and requires appropriate knowledge of the field to be interpreted. Consequently, its outputs are most valuable when integrated with site-specific knowledge and, potentially, other data sources. When applied to coastal environments, in addition to identifying Hi-Var zones that can be translated as shore influence zones (the most active area within the beach), the tool also enables the extraction of two types of shorelines (M1: Shorelines): median and upper shorelines. *SatVar* was tested at locations with different morphological and hydrodynamic characteristics. At the meso and microtidal areas (Sancti-Petri and Narrabeen, respectively), *SatVar* is capable of identifying the upper shoreface as the largest pixel variability area (as conceptually illustrated in Fig. 1). The combination of large tidal ranges and dune mobility in Sefton leads to segmented Hi-Var zones. In all cases, the identified Hi-Var zones correspond to morphological processes described in literature. These may be of interest for future analyses, as they reflect the fact that dynamic change happens across the entire coastal profile. *SatVar* extracted Hi-Var zones that included most shoreline fluctuations over the POI, as suggested by comparisons with SAET and CoastSat extracted shorelines.

SatVar requires site-specific knowledge for the correct interpretation of the output. However, automatic segmentation and the employment of a relatively user-friendly interface in GEE means that the code can be freely accessed and run as many times as desired. Adjusting the POI and AOI are important aspects of the analyses; however, the user should be aware that this may change the number of images that are ultimately used in the collection, as well as the relative pixel values in the variance composite. Although we suggest a POI of 1 year, we argue that the flexibility of changing it opens future applications to shorter time periods (always subject to a sufficiently high number of Sentinel-2 input images being available).

The use of a shore influence zone, together with more traditional shoreline representations of the coast, can enrich our understanding of coastal dynamics. In addition, Hi-Var zones can be used to improve the identification of shoreline positions provided by other SDS algorithms. These algorithms typically rely on some form of guidance to define the search area for the shoreline, such as a manually drawn approximate shoreline (e.g., CoastSat) or a shapefile delineating the beaches (e.g., SAET). Although Sentinel-2 images are only available from 2016, increasing accessibility of medium-resolution satellite images will allow future assessment of the landward and seaward migration of Hi-Var zones. This approach may be particularly useful for understanding shifts in upper shoreface dynamics, intertidal areas, or even dune changes, depending on the site and the objectives of the study. Hi-Var zones in micro and mesotidal environments subject to regular swell waves (such as Narrabeen and Sancti Petri) reflect a variance signal derived from dynamic changes in the surf and swash zones. As the Hi-Var zones also include the submerged part of the beach, new research opportunities, such as the monitoring of nearshore morphologies like the sandbars detected at Sefton, open up.

CRediT authorship contribution statement

Pilar Martín-Gallego: Writing – review & editing, Writing – original draft, Visualization, Validation, Software, Methodology, Investigation, Formal analysis, Conceptualization. **Juan Montes:** Writing – review & editing, Writing – original draft, Visualization, Validation, Software, Methodology, Investigation, Formal analysis, Conceptualization. **Irene Delgado-Fernandez:** Writing – review & editing, Writing – original draft, Project administration, Funding acquisition, Conceptualization. **Laura del Río:** Writing – review & editing, Writing – original draft, Conceptualization. **Theocharis A. Plomaritis:** Writing – review & editing, Project administration, Funding acquisition. **Christopher Marston:** Writing – review & editing, Software.

Declaration of competing interest

The authors declare that they have no known competing financial interests or personal relationships that could have appeared to influence the work reported in this paper.

Acknowledgments

This work is a contribution to MODUL (ProyExcel_00995; PAIDI2020 of Junta de Andalucía, Spain); SCALE (PID2023-151712OB-I00; Ministerio de Ciencia, Innovación y Universidades, Spain); FEDER-UCA-2024-A1-27 (FEDER Andalucía 2021-2027 and Consejería de Universidad, Investigación e Innovación de la Junta de Andalucía, Spain); and the PAI research group RNM-328 (Junta de Andalucía, Spain). Juan Montes was supported by a postdoctoral contract (DGP_POST_2024_00910) funded by Junta de Andalucía (Consejería de Universidad, Investigación e Innovación, Spain, and ESF +, EU).

Appendix

.

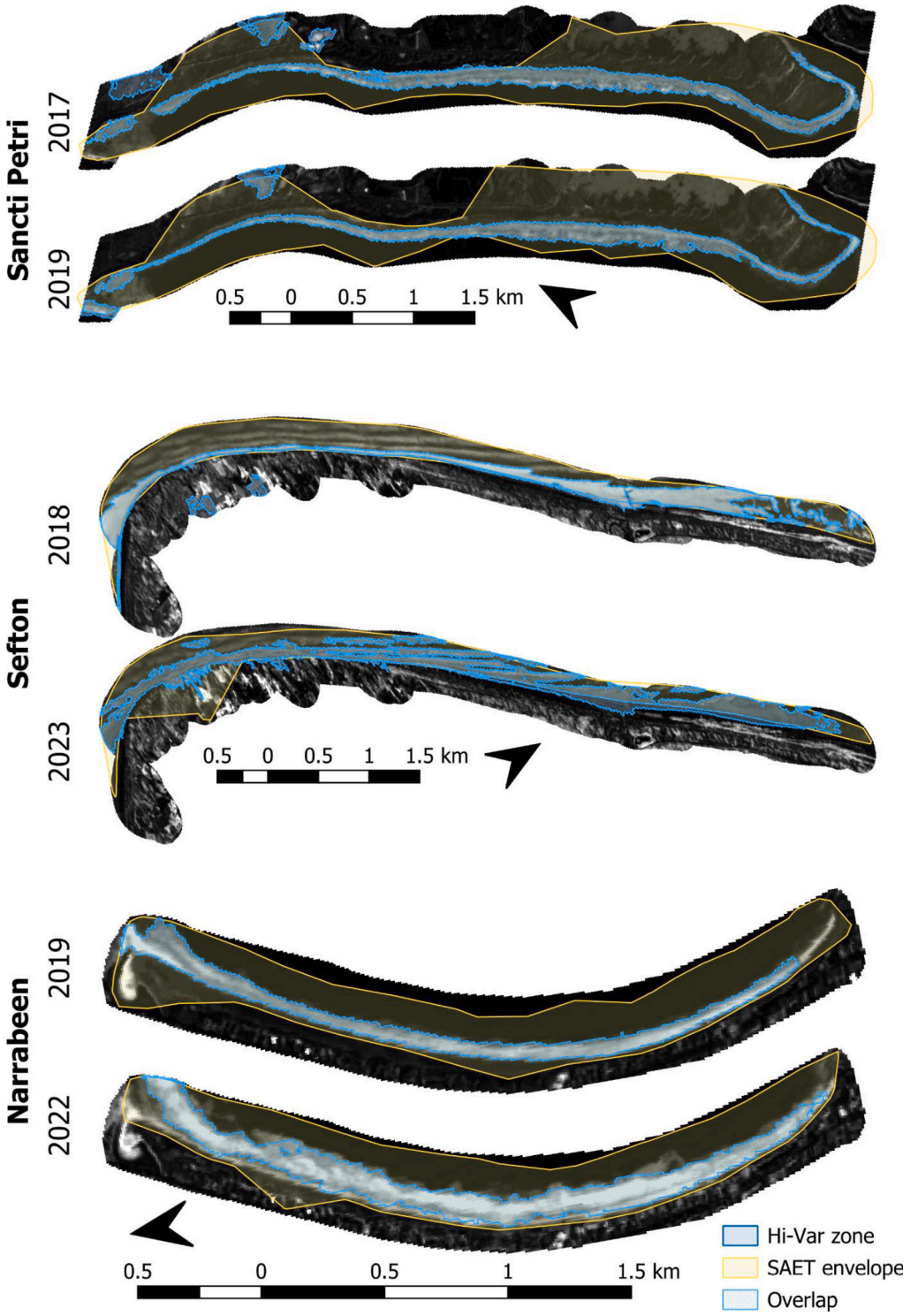


Fig. A1. Comparison between SAET shorelines envelope polygons and Hi-Var zones for performance assessment in the three study sites.

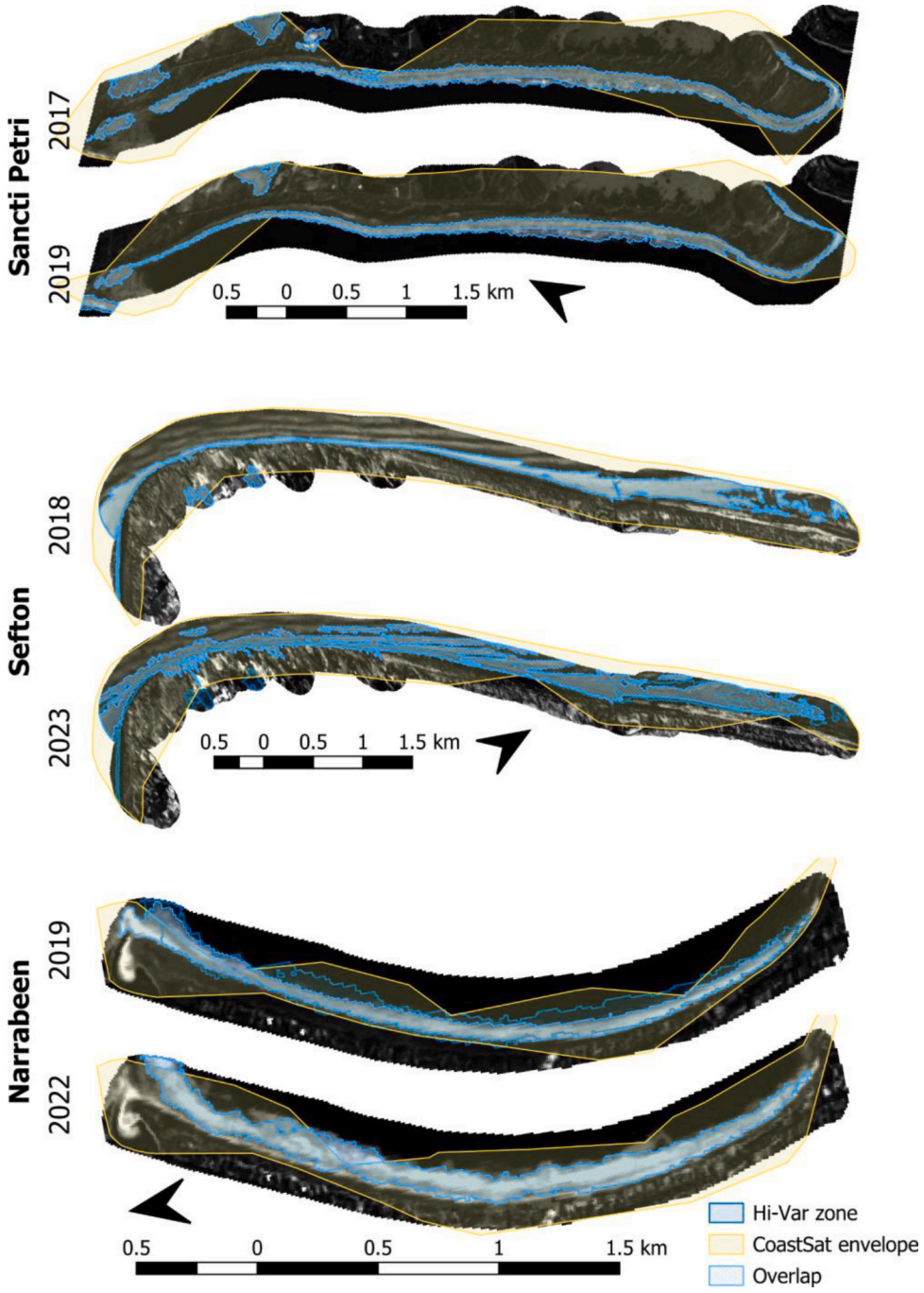


Fig. A2. Comparison between CoastSat shorelines envelope polygons and Hi-Var zones for performance assessment in the three study sites.

Table A.1
Yearly overlap between Hi-Var area and SAET/CoastSat envelope polygon, and commission and omission errors when comparing the Hi-Var area with the SAET/CoastSat envelope polygon.

Study area	Year	Overlap Hi-Var zone − SAET envelope (%)	Hi-Var zone commission error (SAET) (%)	Hi-Var zone omission error (SAET) (%)	Overlap Hi-Var zone − CoastSat envelope (%)	Hi-Var zone commission error (CoastSat) (%)	Hi-Var zone omission error (CoastSat) (%)
Sancti	**2017**	85.14	14.86	79.94	88.01	11.99	81.69
Petri	**2019**	95.06	4.94	84.24	77.48	22.52	87.18
Sefton	**2018**	83.42	16.58	69.77	96.98	3.02	85.64

(*continued on next page*)

Table A.1 (*continued*)

Study area	Year	Overlap Hi-Var zone — SAET envelope (%)	Hi-Var zone commission error (SAET) (%)	Hi-Var zone omission error (SAET) (%)	Overlap Hi-Var zone — CoastSat envelope (%)	Hi-Var zone commission error (CoastSat) (%)	Hi-Var zone omission error (CoastSat) (%)
	2023	83.63	16.37	54.35	99.86	0.14	74.57
Narrabeen	**2019**	99.70	0.30	75.43	88.58	11.42	74.91
	2022	99.69	0.31	64.16	91.72	8.28	72.34
	MEAN	**91.11**	**8.89**	**71.32**	**90.44**	**9.56**	**79.39**

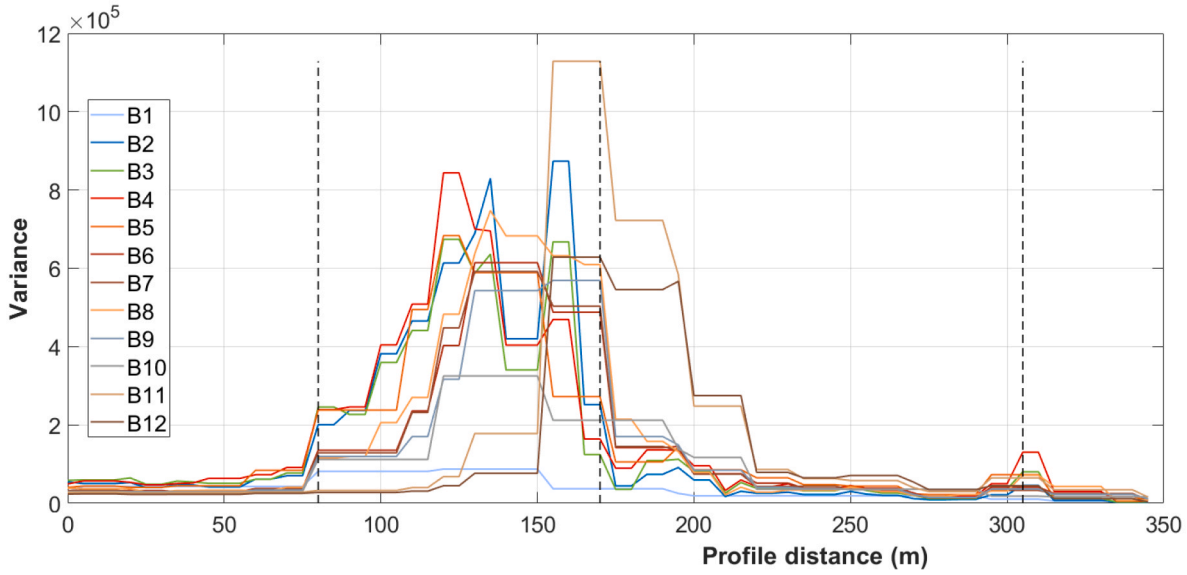


Fig. A3. Variance profiles of all Sentinel-2 bands over a section of Sancti Petri sandspit (defined in Fig. 13), clearly showing the limits of the surf zone (beginning and end) and a distinct peak in variability associated with the dune area.

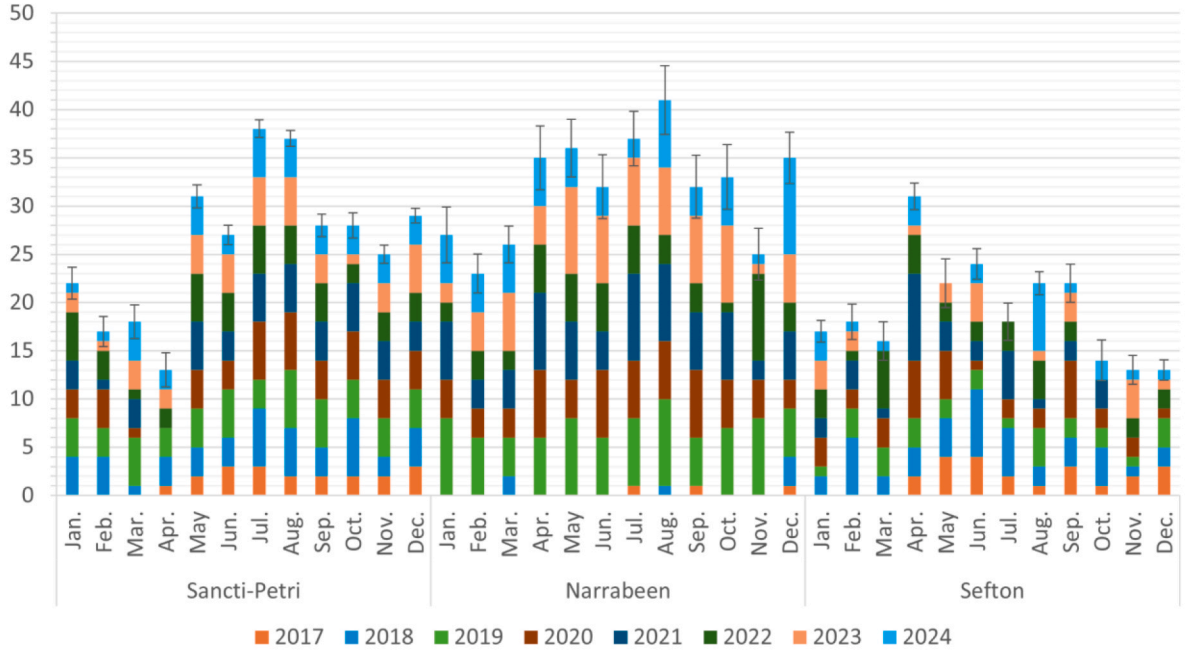


Fig. A4. Date distribution of the images in the GEE collections.

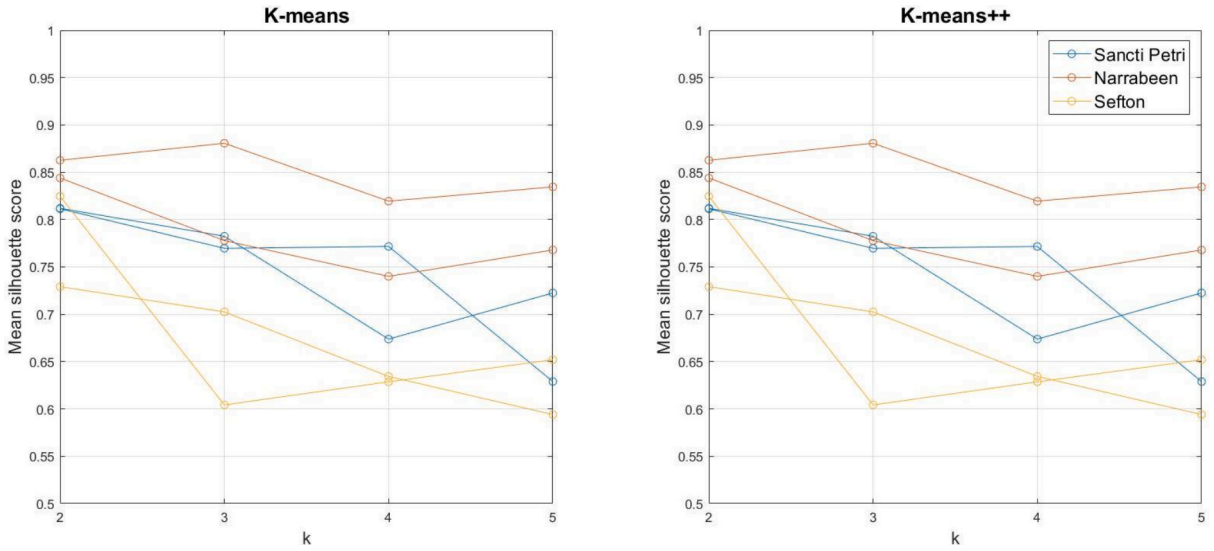


Fig. A5. Silhouette score for k-means and k-means++ for different values of k for the years used to assess the consistency of SatVar performance with other tools. The analysis was repeated 50 times for each year and initialization method to assess the sensitivity of the clustering results to initialization.

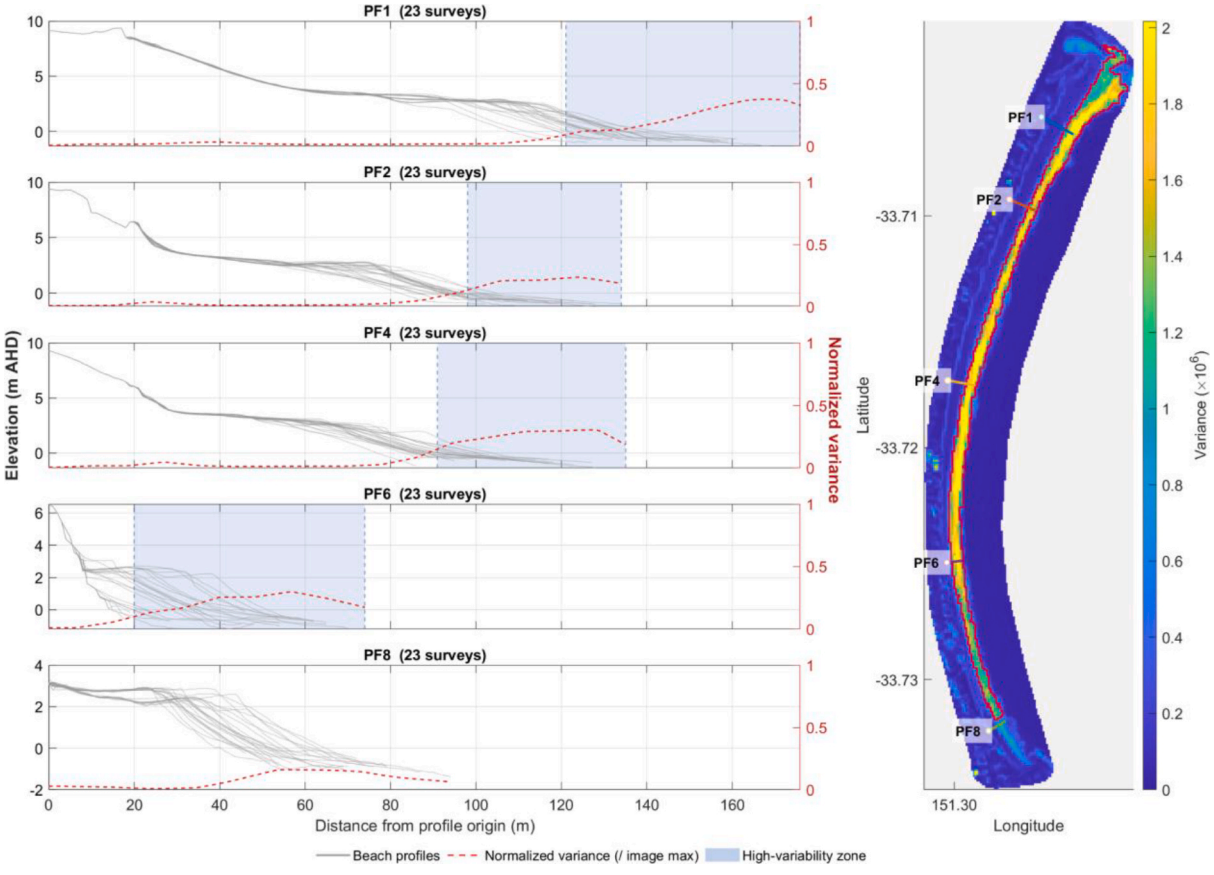


Fig. A6. Comparison between field-surveyed cross-shore beach profiles from and the SatVar Hi-Var zones at Narrabeen for 2019. The dashed red line (right axis) shows the SatVar normalized variance signal along each profile. The Hi-Var zone was extracted using Kmeans with K = 2. Note that the in-situ observations do not include the submerged portion of the beach profiles and may be subject to georeferencing errors.

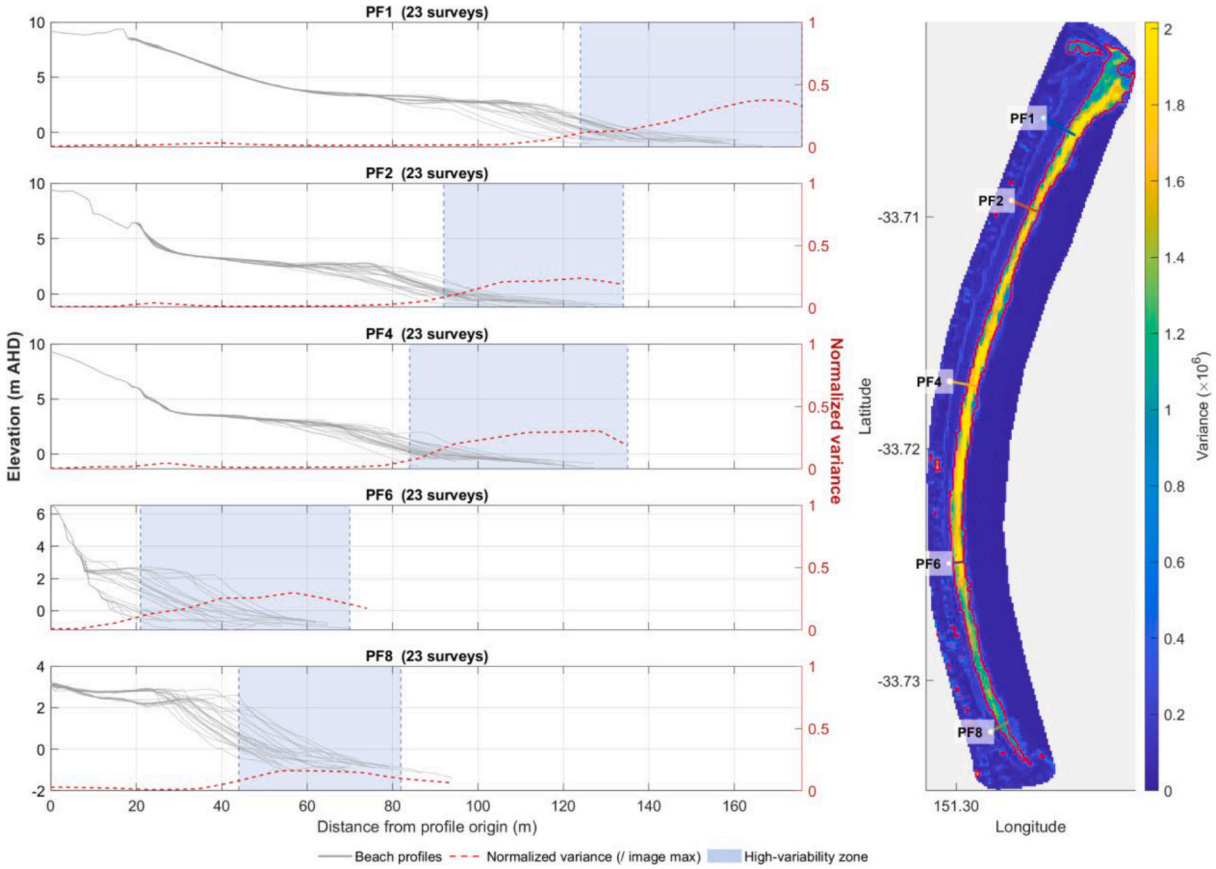


Fig. A7. Comparison between field-surveyed cross-shore beach profiles from Turner et al. (2016) and the SatVar Hi-Var zones at Narrabeen for 2019. The dashed red line (right axis) shows the SatVar normalized variance signal along each profile. The Hi-Var zone was extracted using Kmeans with K = 3 and merging the two clusters with the highest variability. Note that the in-situ observations do not include the submerged portion of the beach profiles and may be subject to georeferencing errors.

Data availability

Google Earth Engine code and user guide: https://doi.org/10.5281/zenodo.17898098.

References

Aghdami-Nia, M., Shah-Hosseini, R., Rostami, A., Homayouni, S., 2022. Automatic coastline extraction through enhanced sea-land segmentation by modifying Standard U-Net. Int. J. Appl. Earth Obs. Geoinf. 109, 102785. https://doi.org/10.1016/j.jag.2022.102785.

Almeida, L.P., Efraim de Oliveira, I., Lyra, R., Scaranto Dazzi, R.L., Martins, V.G., da Fontoura, H., Klein, A., 2021. Coastal Analyst System from Space Imagery Engine (CASSIE): Shoreline management module. Environ. Model. Software 140, 105033. https://doi.org/10.1016/j.envsoft.2021.105033.

Almonacid-Caballer, J., Sánchez-García, E., Pardo-Pascual, J.E., Balaguer-Beser, A.A., Palomar-Vázquez, J., 2016. Evaluation of annual mean shoreline position deduced from Landsat imagery as a mid-term coastal evolution indicator. Mar. Geol. 372, 79–88. https://doi.org/10.1016/j.margeo.2015.12.015.

Arthur, D., Vassilvitskii, S., 2007. k-means++: The Advantages of Careful Seeding. Technical report. Stanford. http://ilpubs.stanford.edu:8090/778/1/2006-13.pdf.

Benavente, J., Del Río, L., Plomaritis, T.A., Menapace, W., 2013. Impact of coastal storms in a sandy barrier (Sancti Petri, Spain). J. Coast. Res. SI65, 666–671. https://doi.org/10.2112/SI65-113.1.

Billet, C., Alonso, G., Danieli, G., Dragani, W., 2024. Evaluation of beach nourishment in Mar del plata, Argentina: an application of the CoastSat toolkit. Coast. Eng. 193, 104593. https://doi.org/10.1016/j.coastaleng.2024.104593.

Bishop-Taylor, R., Nanson, R., Sagar, S., Lymburner, L., 2021. Mapping Australia's dynamic coastline at mean sea level using three decades of Landsat imagery. Remote Sens. Environ. 267, 112734. https://doi.org/10.1016/j.rse.2021.112734.

Boak, E.H., Turner, I.L., 2005. Shoreline definition and detection: a review. J. Coast. Res. 214, 688–703. https://doi.org/10.2112/03-0071.1.

Cabezas-Rabadán, C., Almonacid-Caballer, J., Benavente, J., Castelle, B., Del Río, L., Montes, J., Palomar-Vázquez, J., Pardo-Pascual, J.E., 2024. Assessing Satellite-Derived Shoreline Detection on a Mesotidal Dissipative Beach. Remote Sens. (Basel) 16, 617. https://doi.org/10.3390/rs16040617.

Chen, Y., Kirwan, M.L., 2022. A phenology-and trend-based approach for accurate mapping of sea-level driven coastal forest retreat. Remote Sens. Environ. 281, 113229. https://doi.org/10.1016/j.rse.2022.113229.

Chen, C., Liang, J., Xie, F., Hu, Z., Sun, W., Yang, G., Zhang, Z., 2022. Temporal and spatial variation of coastline using remote sensing images for Zhoushan archipelago, China. Int. J. Appl. Earth Obs. Geoinf. 107, 102711. https://doi.org/10.1016/j.jag.2022.102711.

Copernicus Land Monitoring Service, 2021. Coastal Zones Land Cover/Land Use 2018 (vector), Europe, 6-yearly, Feb. 2021. Doi:10.2909/205e2db2-4e35-4b1b-bf84-271c4a82248c.

Curoy, J., Ward, R.D., Barlow, J., Moses, C., Nakhapakorn, K., 2022. Coastal dynamism in Southern Thailand: an application of the CoastSat toolkit. PLoS One 17 (8), e0272977. https://doi.org/10.1371/journal.pone.0272977.

Davidson-Arnott, R.G., Bauer, B.O., 2021. Controls on the geomorphic response of beach-dune systems to water level rise. J. Great Lakes Res. 47 (6), 1594–1612. https://doi.org/10.1016/j.jglr.2021.05.006.

Davidson-Arnott, R., Bauer, B. and Houser, C. (2010) Introduction to Coastal Processes and Geomorphology. Cambridge: Cambridge University Press.

Delgado-Fernandez, I., O'Keeffe, N., Davidson-Arnott, R.G., 2019. Natural and human controls on dune vegetation cover and disturbance. Sci. Total Environ. 672, 643–656. https://doi.org/10.1016/j.scitotenv.2019.03.494.

Del Río, L., Plomaritis, T.A., Benavente, J., Valladares, M., Ribera, P., 2012. Establishing storm thresholds for the Spanish Gulf of Cádiz coast. Geomorphology 143, 13–23. https://doi.org/10.1016/j.geomorph.2011.04.048.

Dissanayake, P., Brown, J., Karunarathna, H., 2014. Modelling storm-induced beach/dune evolution: Sefton coast, Liverpool Bay, UK. Mar. Geol. 357, 225–242. https://doi.org/10.1016/j.margeo.2014.07.013.

Donchyts, G., Baart, F., Winsemius, H., Gorelick, N., Kwadijk, J., van de Giesen, N., 2016. Earth's surface water change over the past 30 years. Nat. Clim. Chang. 6, 810–813. https://doi.org/10.1038/nclimate3111.

Esteves, L.S., Brown, J.M., Williams, J.J., Lymbery, G., 2012. Quantifying thresholds for significant dune erosion along the Sefton Coast, Northwest England. Geomorphology 143, 52–61. https://doi.org/10.1016/j.geomorph.2011.02.029.

Farris, A.S., Defne, Z., Ganju, N.K., 2019. Identifying salt marsh shorelines from remotely sensed elevation data and imagery. Remote Sens. (Basel) 11 (15), 1795. https://doi.org/10.3390/rs11151795.
Fernández-Montblanc, T., Izquierdo, A., Quinn, R., Bethencourt, M., 2018. Waves and wrecks: a computational fluid dynamic study in an underwater archaeological site. Ocean Eng. 163, 232–250. https://doi.org/10.1016/j.oceaneng.2018.05.062.
Fletcher, C., Rooney, J., Barbee, M., Lim, S., Richmond, B.M., 2003. Mapping shoreline change using digital ortophotogrammetry on Maui. Hawaii. Journal of Coastal Research SI38, 106–124. https://www.jstor.org/stable/25736602.
Frugier, S., Almar, R., Bergsma, E., Granjou, A., 2025. SBI: a sandbar extraction spectral index for multi-spectral satellite optical imagery. Coast. Eng. 200, 104752. https://doi.org/10.1016/j.coastaleng.2025.104752.
Gorelick, N., Hancher, M., Dixon, M., Ilyushchenko, S., Thau, D., Moore, R., 2017. Google Earth Engine: Planetary-scale geospatial analysis for everyone. Remote Sens. Environ. 202, 18–27. https://doi.org/10.1016/j.rse.2017.06.031.
Graffin, M., Touzé, T., Bergsma, E.W., Almar, R., 2025. Towards a global assessment of sandy shorelines: Systematic extraction and validation of optical satellite-derived coastal indicators at various sites. Remote Sens. Environ. 331, 115033. https://doi.org/10.1016/j.rse.2025.115033.
Hagenaars, G., de Vries, S., Luijendijk, A.P., de Boer, W.P., Reniers, A.J.H.M., 2018. On the accuracy of automated shoreline detection derived from satellite imagery: a case study of the sand motor mega-scale nourishment. Coast. Eng. 133, 113–125. https://doi.org/10.1016/j.coastaleng.2017.12.011.
Harley, M.D., Turner, I.L., Short, A.D., Ranasinghe, R., 2009. Interannual variability and controls of the Sydney wave climate. Int. J. Climatol. 30 (9), 1322–1335. https://doi.org/10.1002/joc.1962.
Harley, M.D., Turner, I.L., Short, A.D., Ranasinghe, R., 2011. A reevaluation of coastal embayment rotation: the dominance of cross-shore versus alongshore sediment transport processes, Collaroy-Narrabeen Beach, southeast Australia. J. Geophys. Res. Earth 116 (F4). https://doi.org/10.1029/2011JF001989.
Houser, C., Hapke, C., Hamilton, S., 2008. Controls on coastal dune morphology, shoreline erosion and barrier island response to extreme storms. Geomorphology 100 (3–4), 223–240. https://doi.org/10.1016/j.geomorph.2007.12.007.
Hung, H.T., Tsai, Y.L.S., 2026. NatShore: Automated nation-scale shoreline extraction and change analysis using multidecadal cross-mission remote sensing data. Int. J. Appl. Earth Obs. Geoinf. 149, 105277. https://doi.org/10.1016/j.jag.2026.105277.
Ibaceta, R., Harley, M.D., Turner, I.L., Splinter, K.D., 2023. Interannual variability in dominant shoreline behaviour at an embayed beach. Geomorphology 108706. https://doi.org/10.1016/J.GEOMORPH.2023.108706.
Luijendijk, A., Hagenaars, G., Ranasinghe, R., Baart, F., Donchyts, G., Aarninkhof, S., 2018. The State of the World's Beaches. Sci. Rep. 8, 6641. https://doi.org/10.1038/s41598-018-24630-6.
Mao, Y., Harris, D.L., Xie, Z., Phinn, S., 2021. Efficient measurement of large-scale decadal shoreline change with increased accuracy in tide-dominated coastal environments with Google Earth Engine. ISPRS J. Photogramm. Remote Sens. 181, 385–399. https://doi.org/10.1016/j.isprsjprs.2021.09.021.
Marston, C.G., O'Neil, A.W., Morton, R.D., Wood, C.M., Rowland, C.S., 2023. LCM2021 – the UK Land Cover Map 2021. Earth Syst. Sci. Data 15, 4631–4649. https://doi.org/10.5194/essd-15-4631-2023.
Martín-Gallego, P., Delgado-Fernandez, I., Marston, C., 2025. The application of satellite remote sensing to coastal dune environments: a systematic review. Prog. Phys. Geogr.: Earth Environ. https://doi.org/10.1177/03091333251380450.
McFeeters, S.K., 1996. The use of the Normalized Difference Water Index (NDWI) in the delineation of open water features. Int. J. Remote Sens. 17 (7), 1425–1432. https://doi.org/10.1080/01431169608948714.
Montes, C., Benavente, J., Puig, M., Montes, J., Talavera, L., Plomaritis, T.A., 2024. High-Resolution Interannual Evolution of the Dune Toe at a Mesotidal Barrier (Camposoto Beach, SW Spain). Journal of Marine Science and Engineering 12, 718. https://doi.org/10.3390/jmse12050718.
Moore, L.J., 2000. Shoreline mapping techniques. J. Coast. Res. 16 (1), 111–124. https://journals.flvc.org/jcr/article/view/80780.
Nasir, F., Roslee, A., Zakaria, J., Ariffin, E.H., Mokhtar, N.A., 2022. Shoreline identification bias: theoretical and measured value for meso-tidal beaches in Kuala Nerus, Terengganu (Malaysia). J. Mar. Sci. Appl. 21 (3), 184–192. https://doi.org/10.1007/s11804-022-00293-8.
Pajak, M.J., Leatherman, S.P., 2002. The high-water line as shoreline indicator. J. Coast. Res. 18 (1), 92–107. https://journals.flvc.org/jcr/article/view/81276.
Palomar-Vázquez, J., Pardo-Pascual, J.E., Almonacid-Caballer, J., Cabezas-Rabadán, C., 2023. Shoreline Analysis and Extraction Tool (SAET): a New Tool for the Automatic Extraction of Satellite-Derived Shorelines with Subpixel Accuracy. Remote Sens. (Basel) 15, 3198. https://doi.org/10.3390/rs15123198.
Pardo-Pascual, J.E., Almonacid-Caballer, J., Ruiz, L.A., Palomar-Vázquez, J., 2012. Automatic extraction of shorelines from Landsat TM and ETM+ multi-temporal images with subpixel precision. Remote Sens. Environ. 123, 1–11. https://doi.org/10.1016/j.rse.2012.02.024.
Pasquarella, V.J., Brown, C.F., Czerwinski, W., Rucklidge, W.J., 2023. Comprehensive Quality Assessment of Optical Satellite Imagery Using Weakly Supervised Video Learning. Presented at the Proceedings of the IEEE/CVF Conference on Computer Vision and Pattern Recognition, pp. 2125–2135.
Poizot, E., Anfuso, G., Méar, Y., Bellido, C., 2013. Confirmation of beach accretion by grain-size trend analysis: Camposoto beach, Cádiz, SW Spain. Geo-Mar. Lett. 33, 263–272. https://doi.org/10.1007/s00367-013-0325-3.
Puig, M., Del Río, L., Plomaritis, T.A., Benavente, J., 2016. Contribution of storms to shoreline changes in mesotidal dissipative beaches: case study in the Gulf of Cádiz (SW Spain). Nat. Hazards Earth Syst. Sci. 16, 2543–2557. https://doi.org/10.5194/nhess-16-2543-2016.
Pye, K., Blott, S.J., 2008. Decadal-scale variation in dune erosion and accretion rates: an investigation of the significance of changing storm tide frequency and magnitude on the Sefton coast. UK. Geomorphology 102 (3–4), 652–666. https://doi.org/10.1016/j.geomorph.2008.06.011.
Sánchez-García, E., Palomar-Vázquez, J.M., Pardo-Pascual, J.E., Almonacid-Caballer, J., Cabezas-Rabadán, C., Gómez-Pujol, L., 2020. An efficient protocol for accurate and massive shoreline definition from mid-resolution satellite imagery. Coast. Eng. 160, 103732. https://doi.org/10.1016/j.coastaleng.2020.103732.
Sherman, D.J., Bauer, B.O., 1993. Dynamics of beach-dune systems. Prog. Phys. Geogr.: Earth Environ. 17 (4), 413–447. https://doi.org/10.1177/030913339301700402.
Short, A.D., Hesp, P.A., 1982. Wave, beach and dune interactions in South Eastern Australia. Mar. Geol. 48, 259–284.
Smith, A., Houser, C., Lehner, J., George, E., Lunardi, B., 2020. Crowd-sourced identification of the beach-dune interface. Geomorphology 367, 107321. https://doi.org/10.1016/j.geomorph.2020.107321.
Splinter, K.D., Turner, I.L., Davidson, M.A., Barnard, P., Castelle, B., Oltman-Shay, J., 2014. A generalized equilibrium model for predicting daily to interannual shoreline response. J. Geophys. Res. Earth 119, 1936–1958. https://doi.org/10.1002/2014jf003106.
Splinter, K.D., Harley, M.D., Turner, I.L., 2018. Remote sensing is changing our view of the coast: Insights from 40 years of monitoring at Narrabeen- Collaroy. Australia. Remote Sensing 10, 1744. https://doi.org/10.3390/rs10111744.
Talavera, L., Del Río, L., Benavente, J., Barbero, L., López-Ramírez, J.A., 2018. UAS as tools for rapid detection of storm-induced morphodynamic changes at Camposoto beach, SW Spain. Int. J. Remote Sens. 39, 5550–5567. https://doi.org/10.1080/01431161.2018.1471549.
Trenhaile, A.S., 1987. The Geomorphology of Rock Coasts. Oxford: Clarendon Press.
Turner, I.L., Harley, M.D., Short, A.D., Simmons, J.A., Bracs, M.A., Phillips, M.S., Splinter, K.D., 2016. A multi-decade dataset of monthly beach profile surveys and inshore wave forcing at Narrabeen. Australia. Scientific Data 3 (1), 1–13. https://doi.org/10.1038/sdata.2016.24.
Vitousek, S., Buscombe, D., Vos, K., Barnard, P.L., Ritchie, A.C., Warrick, J.A., 2023. The future of coastal monitoring through satellite remote sensing. Cambridge Prisms: Coastal Futures 1, e10.
Vos, K., Splinter, K.D., Harley, M.D., Simmons, J.A., Turner, I.L., 2019. CoastSat: a Google Earth Engine-enabled Python toolkit to extract shorelines from publicly available satellite imagery. Environ. Model. Softw. 122, 104528. https://doi.org/10.1016/j.envsoft.2019.104528.
Vos, K., Splinter, K.D., Palomar-Vázquez, J., Pardo-Pascual, J.E., Almonacid-Caballer, J., Cabezas-Rabadán, C., Kras, E.C., Luijendijk, A.P., Calkoen, F., Almeida, L.P., Pais, D., Klein, A.H.F., Mao, Y., Harris, D., Castelle, B., Buscombe, D., Vitousek, S., 2023. Benchmarking satellite-derived shoreline mapping algorithms. Commun. Earth Environ. 4, 1–17. https://doi.org/10.1038/s43247-023-01001-2.
Vousdoukas, M.I., Ferreira, P.M., Almeida, L.P., Dodet, G., Psaros, F., Andriolo, U., Taborda, R., Silva, A.N., Ruano, A., Ferreira, Ó.M., 2011. Performance of intertidal topography video monitoring of a meso-tidal reflective beach in South Portugal. Ocean Dyn. 61, 1521–1540. https://doi.org/10.1007/s10236-011-0440-5.
Woodroffe, C.D., Rogers, K., McKee, K.L., Lovelock, C.E., Mendelssohn, I.A., Saintilan, N., 2016. Mangrove sedimentation and response to relative sea-level rise. Ann. Rev. Mar. Sci. 8, 243–266. https://doi.org/10.1146/annurev-marine-122414-034025.
Zhang, B., Chang, L., Wang, Z., Wang, L., Ye, Q., Stein, A., 2025. Multi-decadal dutch coastal dynamic mapping with multi-source remote sensing imagery. Int. J. Appl. Earth Obs. Geoinf. 138, 104452. https://doi.org/10.1016/j.jag.2025.104452.